Available online at www.sciencedirect.com
ScienceDirect
Coordination Chemistry Reviews 251 (2007) 328–350
COORDINATION CHEMISTRY REVIEWS
www.elsevier.com/locate/ccr

Review

Charge transfer-excited state emission spectra of mono- and bi-metallic coordination complexes: Band shapes, reorganizational energies and lifetimes

John F. Endicott [a,*], Yuan-Jang Chen [b]

[a] *Department of Chemistry, Wayne State University, Detroit, MI 48202-3489, USA*
[b] *Department of Chemistry, Fu Jen Catholic University, Taipei Hsien 24205, Taiwan, ROC*

Received 20 March 2006; accepted 21 July 2006
Available online 18 August 2006

Contents

* Corresponding author. Tel.: +1 3135772607; fax: +1 3135778822.
E-mail address: jfe@chem.wayne.edu (J.F. Endicott).

0010-8545/$ – see front matter
doi:10.1016/j.ccr.2006.07.021

Abstract

The low energy sidebands of an emission spectrum contain information about the difference between the ground and the excited state molecular structures. The structural information that can be extracted from the sideband intensities and structure decreases as the component bandwidths increase, but there is significant structural information in the sidebands of the charge transfer emission spectra of even the relatively broad ($\Delta\nu_{1/2} \sim 1000\,cm^{-1}$) charge transfer (CT) emission spectra of transition metal complexes in frozen solutions. A Gaussian band shape model for the contributions of vibronic components is described and applied to the analysis of transition metal CT emission band shapes in frozen solution. The uncertainties of this approach are examined with respect to the emission spectra calculated from reported resonance-Raman (rR) parameters; such calculated spectra reproduce the frozen solution emission spectra of $[Ru(bpy)_3]^{2+}$ and $[Ru(NH_3)_4bpy]^{2+}$ very well. Patterns of excited state distortions can be expressed in terms of variations in the vibrational reorganizational energies, λ_k (proportional to the squared displacements), of the normal modes that correlate with the differences in excited and ground state geometries. The excited state distortions usually correspond to displacements in a large number of ground state molecular vibrational modes (more than 11 for the Ru–bpy complexes), and the bandwidths characteristic of CT spectra in frozen solutions preclude their resolution in frozen solution spectra. Thus, the convolution of the overlapping spectral contributions of these individual distortion modes results in a vibronic sideband that is broad and sometimes weakly structured, and the variations of the sideband amplitude provides information about variations in molecular structure for a series of closely related complexes. The emission sidebands can readily be converted into a reorganizational energy profile (emrep) in which the variations in amplitude are more readily interpreted in terms of molecular distortions and in which the contributions from the distortions in the highest frequency vibrational modes are more evident. This approach has been used to analyze the patterns of variations of the vibronic sideband structure of the frozen solution CT emission spectra of $[Ru(L)_4bpy]^{2+}$, $[Ru(bpy)_2PP]^{2+}$, $[\{(bpy)_2Ru\}_2PP]^{4+}$ (bpy, 2,2′-bipyridine; PP, a tetraazapolypyridyl bridging ligand) and cyanide-bridged Cr(III)/Ru(II) complexes. The observed emission energies of the bpy complexes span a range of about $8000\,cm^{-1}$ and the vibronic sideband amplitudes tend to decrease appreciably (over about a two-fold range for the $[Ru(L)_4bpy]^{2+}$ complexes) and systematically with decreasing emission energy in each class of these complexes. This attenuation of the vibronic sideband intensities is ascribed to the increases in ground state–excited state configurational mixing with decreasing energy differences between the states and to the large electronic matrix elements. The variations in emreps also suggest that there is a great deal of excited state–excited state configurational mixing (probably ligand field/metal to ligand CT) in most, but not all, $[Ru(L)_4bpy]^{2+}$ complexes and relatively little such configurational mixing between the different MLCT valence isomer excited states of the $[\{(bpy)_2Ru\}_2PP]^{4+}$ complexes. The comparison of the emreps of NH/ND isotopomers of the $[Ru(L)_4bpy]^{2+}$ and of the cyanide-bridged Cr(III)/Ru(II) complexes has permitted the resolution of the very weak contributions of distortions of the C–H (in the former) and N–H (in the latter) stretching vibrational modes, and it appears that decay pathways that involve only nuclear tunneling in the C–H modes cannot account for the decay behavior of the $[Ru(L)_4bpy]^{2+}$ complexes while such pathways in the N–H modes may account for that of the Cr(III)/Ru(II) complexes.

Keywords: Zero point energy; MLCT; Resonance-Raman rR spectra; Emission spectral band shapes; MMCT; Reorganizational energy profiles; Transition metal complexes; Effects of configurational mixing

1. Introduction

The manipulation of chemical reactivity, the design reagents for specific purposes, etc., depends on knowledge of how the properties of molecules contribute to their reactivity. The simplest class of chemical reactions are those in which a single electron is transferred between donor and acceptor, key electron transfer parameters are often evaluated by means of spectroscopic measurements since it is well known that the same general molecular properties govern thermal electron transfer reactivity of donor–acceptor (D/A) complexes and the absorption of light in the formation of or the emission of light in the relaxation of charge transfer (CT) excited states [1–14]. However, the characterization of the properties CT excited states and of evaluation of key electron transfer parameters is generally difficult at least in part because: (a) transition metal complexes typically have many electronic states that are relatively close in energy and configurational mixing between these states can make the characterization of reactivity patterns difficult; (b) the evaluation of key parameters tends to be model dependent. We have found that emission band shapes can provide useful experimental probes of the variations in key electron transfer properties of related coordination complexes.

The properties that are most important in an electron transfer system are: (a) the zero point energy difference between the initial and final states ($E^{00'}$ or Δzpe); (b) the reorganizational energy associated with the solvent redistribution in the electron transfer process, λ_s; (c) the reorganizational energies associated with the accompanying nuclear displacements within the molecule(s), λ_h; (d) the vibrational frequencies, ν_h, that correspond to those nuclear displacements; (e) the electronic matrix element, H_{if}, that mixes the diabatic configurations of the initial and final electronic states. The comparisons between spectra and electron transfer reactivity in this report are confined to excited state relaxation processes which correspond to electron transfer in the Marcus inverted region [8,15–18]. It is expected that the highest frequency distortion modes dominate the electron transfer reactivity in this regime, in which $E^{00'}$ is much greater than the effective reorganizational energy [16,17,19]; however, many studies of ruthenium and osmium polypyridyl (PP) complexes have implicated the medium frequency PP-ligand skeletal modes as the dominant contributors to the relaxation channels for excited state relaxation [20–26].

The Δzpe may in principle be extracted from absorption and/or emission maxima if the excited state is not very distorted (i.e., for the Huang–Rhys factors, $S_n < 1$). Similarly, the reorganizational energies may in principle be inferred from the absorption and/or emission spectral band shapes. The band shape as used here includes both the intrinsic bandwidth of the spectral components and the deviation (or skewness) of the overall spectral band shape compared to that expected for a single transition component.

It is useful to formulate the changes in observed spectroscopic parameters in terms of idealized initial (or "diabatic") states in which there are no interactions between the D and A components of the coordination complex, and in which it is possible to determine the properties of these parameters. Configurational mixing commingles the properties of the different electronic states, and variations in their spectral manifestations in a series of related complexes can be interpreted in terms of the variations in the extent of configurational mixing among electronic states. This approach is conveniently formulated in terms of the wavefunctions of the various electronic excited states (j) with the ground state (g) where configurational mixing is represented in terms of a normalization factor η_{gs}, a normalized mixing coefficient α_{gj}, and wavefunctions representing the electronic states in the limit of no mixing (designated by the degree superscript) [4]:

$$\Psi_g = \eta_{gs}\Psi_g^\circ + \sum_j \alpha_{gj}\Psi_j^\circ \quad (1)$$

Complexes containing the well-known Ru–bpy chromophore have been used to develop our approaches to band shape analysis, and since spin–orbit coupling (soc) is significant among these complexes, Eq. (1) should be reformulated as

$$^1\Psi_g = \eta_{gs}^{(1)1}\Psi_g^\circ + \sum_j \alpha_{gj}^{(1,1)1}\Psi_j^\circ + \sum_k \alpha_{kg}^{(1,3)3}\Psi_j^\circ \quad (2)$$

where the left superscripts designate the spin multiplicity of the electronic state and the superscripts (M_s, M_s) and (M_s, $M_s \pm 2$), of the mixing coefficients distinguish between the spin allowed and the soc-promoted configurational mixings, respectively. One generally expects that $\alpha_{gj}^{(1,1)} > \alpha_{kg}^{(1,3)}$ and the soc-promoted mixings will only be considered for the lowest energy excited state. Furthermore, the coefficients for mixing the higher energy excited states with the ground state are much smaller than those for excited state/excited state configurational mixing, and ground state properties are relatively insensitive to their variations so that Eq. (2) may be simplified:

$$^1\Psi_g(\text{eff}) \cong \eta_{gs}^{(1)1}\Psi_g^\circ(\text{eff}) + \alpha_{ge}^{(1,1)1}\Psi_e^m + \alpha_{ge}^{(1,3)3}\Psi_e^m \quad (3)$$

For example, $^1\Psi_e^m$ and $^3\Psi_e^m$ may be identified with the lowest energy metal-to-ligand CT (MLCT) excited states with singlet (^{1}MLCT) and triplet (^{3}MLCT) spin multiplicity, respectively, after mixing with other excited states. In our discussions of the lowest energy ^{3}MLCT excited states of Ru–polypyridyl (Ru–PP) complexes, we will consider configurational mixings among the triplet excited states but only of the lowest energy ^{3}MLCT excited state with the ground state so that the effective excited state wavefunction becomes:

$$^3\Psi_e = \eta_{es}^{(3)3}\Psi_e^\circ + \sum_k \alpha_{ek}^{(3,3)3}\Psi_k^\circ - \alpha_{eg}^{(3,1)1}\Psi_g^\circ$$
$$\approx \eta_{es}^{(3')3}\Psi_e^m - \alpha_{eg}^{(3,1)1}\Psi_g^\circ \quad (4)$$

Likely candidates for mixing with the lowest energy excited state are higher energy excited states (k) of the types: (a) other CT excited states (e.g., ^{3}MLCT′); (b) metal-centered ligand field Ru^{II} (^{3}LF); (c) ligand-centered ($^3\pi\pi^*$); (d) ligand-to-ligand charge transfer (^{3}LLCT) excited states. Our recent studies have examined the first and implicated the second of these higher energy excited states in modifying the properties of the lowest energy ^{3}MLCT excited states of Ru^{II}–polypyridyl complexes.

The ambient absorption and emission spectra of D/A complexes in solution tend to be broad and structureless as a consequence of the combination of intrinsically large component bandwidths (typical values of $\Delta\nu_{1/2} \sim 2000\,cm^{-1}$ for complexes discussed in this review) and extracting the parameters of interest from these spectra can be especially difficult. Furthermore, the observed absorption envelope for transition metal complexes can be convoluted with the contributions of several electronic transitions and there are few quantitative criteria for identifying or separating such contributions. On the other hand, the vibronic parameters, λ_h and ν_h, may often be extracted more readily from the resonance-Raman rR spectra generated by the high intensity excitation of the charge transfer absorption bands [27–30].

Almost all emission spectra correspond to a single electronic transition and, while the ambient emission spectra of CT excited states also tend to be broad and unstructured, the component bandwidths decrease markedly with temperature so that there are corresponding increases in the skewness and resolution of the spectral band shapes at lower temperatures. In the limit of very low temperature (<10 K) and for the emission spectra of D/A complexes doped into single crystals it is possible to resolve the individual contributions of each of the displacement modes [31], but these conditions are not convenient for examining series of related complexes and not possible for some of the compounds

of interest. In contrast, emission spectra of complexes in frozen solutions are relatively easily obtained, and, although the CT emission spectra are still very broad in 77 K frozen solutions, a great deal of useful information about the relevant molecular parameters can be extracted from careful determinations of these spectra and their band shapes [32,33]. Our approaches to the systematic analysis of the band shapes of 77 K frozen solution CT spectra and some recent results are summarized in this report.

2. Summary of the contributions to charge transfer emission band shapes

The characteristic features of an emission spectrum are its energy, intensity (or emission yield), bandwidth and band shape. The emission decay after pulsed excitation yields a characteristic lifetime, τ, or decay rate constant, $k_d = \tau^{-1} = k_r + k_{nr}$ (where k_r and k_{nr} are the radiative and non-radiative relaxation rate constants, respectively).

2.1. Emission intensity

A general expression for the emission intensity at a frequency ν_m is [9,29,30,34]:

$$I_{\nu_m} \cong \frac{64\pi^4}{3h^3c^3 \ln 10} \frac{\nu_m \eta^3 H_{eg}^2 (\Delta\mu_{eg})^2}{(4\pi\lambda_s k_B T)^{1/2}} (\mathrm{FC}) \quad (5)$$

The transition dipole, M_{eg}, has been replaced by $(H_{eg}/h\nu_{eg})\Delta\mu_{eg}$ in Eq. (5) [9,34,35], where ν_m is the frequency of the incident radiation, H_{eg} the electronic matrix element, and $\Delta\mu_{eg}$ is the difference of excited state and ground state dipole moments; this substitution assumes that $H_{eg} \ll h\nu_{eg}$. Other parameters are: η, the index of refraction; λ_s, the reorganizational energy of the solvent and other displacement modes with quanta $h\nu_s < 4k_BT$; c, the speed of light. Based on Gaussian band shapes (see Section 2.2) and a wave packet model and for the contributions of a single vibrational mode (FC) can be represented by [9,29,30]:

$$(\mathrm{FC})_k \cong \sum_j F_{j,k} [e^{-\{4G_j^2 \ln 2/\Delta\nu_{1/2}^2\}}] \quad (6)$$

$$F_{j,k} = \frac{S_k^j e^{-S_k}}{j!}, \quad S_k = \frac{\lambda_k}{h\nu_k} \quad (7)$$

$$G_j = E_{ge}^{0'0} - \lambda_s - jh\nu_k - h\nu_m \quad (8)$$

where for the high frequency vibrational modes $h\nu_k \geq \sim 4k_BT$.

The determination of absolute intensity requires a measurement of the emission yield [36], $\phi_r = k_r\tau$ [37] (ϕ_r is generally $\ll 1$ for the complexes discussed here), but since this article is primarily concerned with emission band shapes and these are independent of the emission yield, we will not deal with this issue. In discussing emission band shapes it is important to note that intensity for the limit in which the donor (D) and acceptor (A) are weakly coupled, as expressed in Eq. (5), is a first order function in ν_m [9]. In a Gaussian analysis of the emission band shape it is necessary to correct for this by dividing the observed intensity by ν_m. As illustrated in Fig. 1, failure to make this correction would underestimate sideband intensities by a few percent. There are some reports in the literature that express I_{ν_m} in terms of M_{eg} and therefore divide the observed intensity by ν_m^3; this corresponds to a limit in which the electron density is delocalized between D and A, and if the D/A coupling is weak this procedure distorts the band shape and overestimates the sideband intensity by 15–25% in the region with energies 1200–1600 cm^{-1} smaller than the band maximum as shown in Fig. 1; intermediate situations have also been treated in the literature [38]. The spectral analysis in this report is based on the limit represented by Eq. (5).

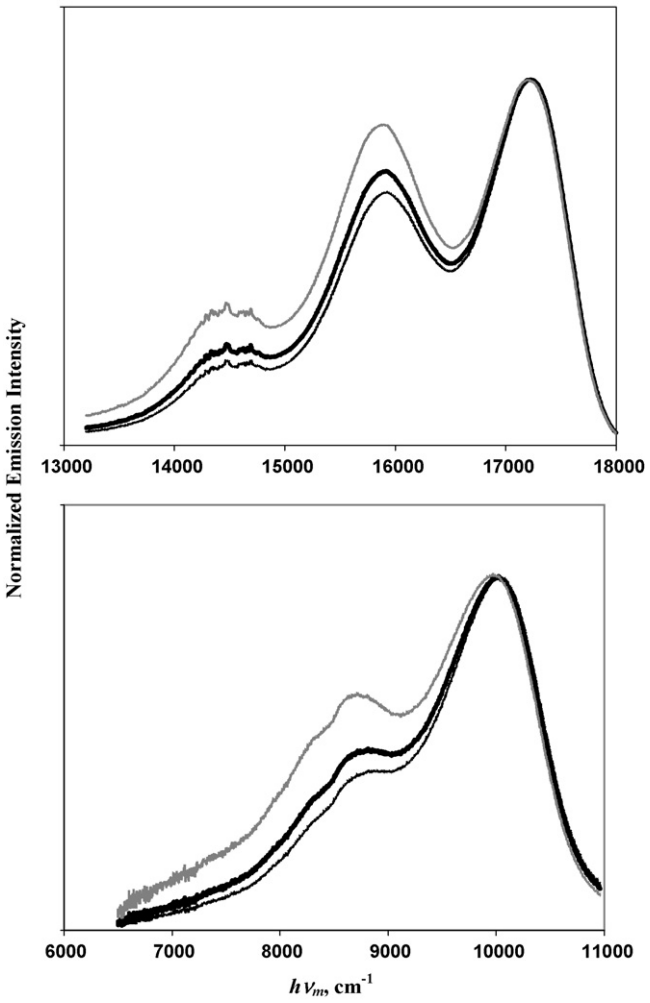

Fig. 1. Emission spectra of $[Ru(bpy)_3]^{2+}$ (top) and $[\{(NH_3)_4Ru\}_2dpp]^{4+}$ (bottom) obtained in 77 K butyronitrile solutions, lower thin black curves. The variations of vibronic intensities with the assumed dependence of the emission intensity on emission frequency are illustrated by: gray curves, I/ν_m^3; heavy black curves, I/ν_m.

2.2. Emission energy: $E^{0'0}$ and the "fundamental" component

The zpe difference between the excited and ground states is generally not the energy maximum of the emission band; for

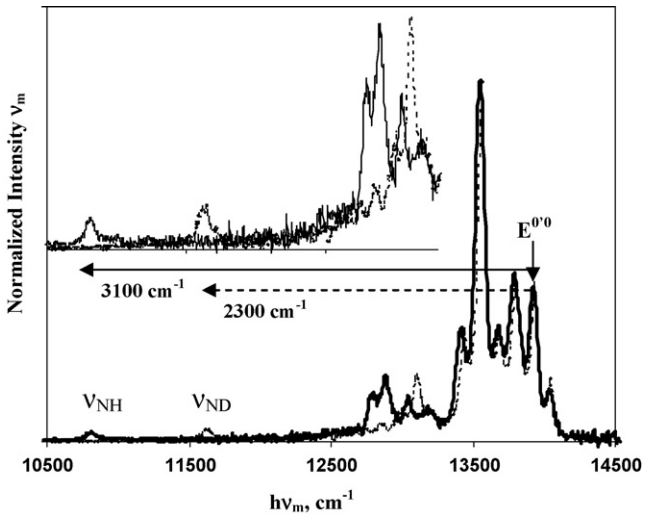

Fig. 2. Emission spectrum of $[Cr([14]aneN_4)(CN)_2]^+$ in butyronitrile glass at 77 K. Solid line for $[Cr([14]aneN_4)(CN)_2]^+$, dotted line for $[Cr(d_4\text{-}[14]aneN_4)(CN)_2]^+$; Chen and Endicott, work in progress; based on Fig. 2 in [50].

example: (a) the $0'0$ transition is formally Laporte forbidden in the LF emission spectra of centrosymmetric complexes (see Fig. 2); (b) the maximum of the envelope that results from the sum of overlapping $E^{0'0}$ and vibronic components in a broad band spectrum is systematically shifted to lower energies as bandwidth increases, as a result of the overlapping component intensity contributions (see Fig. 3).

The $E^{0'0}$ component of the $^2E \rightarrow {}^4A_2$ emission spectrum (O_h notation used for simplicity) of *trans*-$[Cr([14]aneN_4)(CN)_2]^+$ (C_{2h} microsymmetry) in a 77 K frozen butyronitrile solution [39] in Fig. 2 is Laporte forbidden, and therefore weak compared to some of the vibronic components. The weak higher energy (anti-Stokes) component is assigned as a "hot band" (emission from

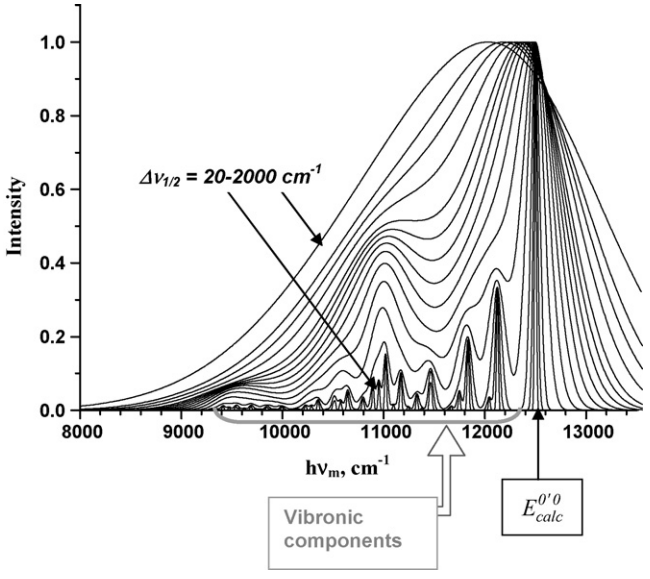

Fig. 3. Emission spectra calculated for $[Ru(NH_3)_4bpy]^{2+}$ [32] based on reported resonance-Raman parameters [40]. Based on Fig. 10 in [32] with $\Delta\nu_{1/2}$ = 20, 50, 100, 200, 300, 400, 500, 600, 700, 800, 900, 1100, 1300, 1500 and 2000 cm^{-1}.

a thermally populated vibrational excited state of the ^2E electronic excited state) and the $E^{0'0}$ band is identified by comparing energy spacings and intensities of the Stokes and anti-Stokes components. That the $E^{0'0}$ component has significant intensity in this complex indicates that the complex is not rigorously centrosymmetric in the frozen solution. The finite bandwidths of the spectral components (~10 cm^{-1}) in this spectrum are a combined consequence of the spectral resolution and the effects of the distribution of environments in solution.

The emission spectra of charge transfer excited states in frozen solutions at 77 K are much broader and the vibronic structure is more poorly resolved (e.g., see Fig. 1) than observed for the d–d spectrum in Fig. 2. This is a consequence of the >100-fold larger bandwidths characteristic of CT excited state emission spectra. These large bandwidths result from: (a) the distribution of different solvent environments of the complexes in solution and the variations in λ_s and $E^{0'0}$ with the solvent environment; (b) overlapping component contributions; (c) contributions of the solvent reorganizational energy, λ_s. For example, the "component" corresponding to $E^{0'0}$ for the emission spectrum of a CT excited state, $E^{0'0}_{obsd}$, is an envelope of the overlapping contributions of the differently solvated complexes in the solution; or, for n_i the number of complexes with the solvent environment i and energy $E_i^{0'0}$, this component can be represented:

$$E^{0'0}_{obsd} = \frac{\sum_i^{\text{all solvates}} n_i E_i^{0'0}}{\sum_i^{\text{all solvates}} n_i} \quad (9)$$

If the distribution of solvates is a statistically normal distribution, then the function $E^{0'0}_{obsd}$ is expected to be nearly Gaussian-shaped.

The shift of the emission maxima shown in Fig. 3 was calculated [32] for $[Ru(NH_3)_4bpy]^{2+}$ based on rR parameters [40], and this shift occurs only because more vibronic components overlap with $E^{0'0}$ for each increase of the bandwidth. For $\Delta\nu_{1/2} < 500$ cm^{-1}, $E_{max(calc)} \approx (E^{0'0} + 0)$ cm^{-1}, but for $\Delta\nu_{1/2} = 1000$ cm^{-1}, $E_{max(calc)} \approx (E^{0'0} + 114)$ and $(E^{0'0} + 143)$ cm^{-1}, respectively for $[Ru(bpy)_3]^{2+}$ and $[Ru(NH_3)_4bpy]^{2+}$ (see Fig. 4); for ambient solution conditions $\Delta\nu_{1/2} \approx 2000$ cm^{-1} and $(E_{max(calc)} - E^{0'0}) \approx 440$ and 630 cm^{-1}, respectively. More generally for $\Delta\nu_{1/2} > 500$ cm^{-1}:

$$h\nu_{max(emis)} \cong E^{0'0} - a\Delta\nu_{1/2} + b \quad (10)$$

Since the values of "a" and "b" in the correlations in Fig. 4 are determined only by the values of $h\nu_h$ and S_h for the vibronic components, and since these vary from one complex to another, the values of "a" and "b" are variables characteristic of the different vibronic structure of each complex. This effect does not make a very large contribution to $E^{0'0}_{obsd}$ in spectra obtained in 77 K glasses, but for ambient solution conditions it contributes significantly to poor spectral resolution and to an ambiguous identification of $E^{0'0}$. Nevertheless, highest energy components deconvoluted from the 77 K emission spectra will also contain some contributions from vibronic overlap when some $h\nu_h$ are less than $\Delta\nu_{1/2}$. As a consequence, these components are referred to as the "fundamentals" (f).

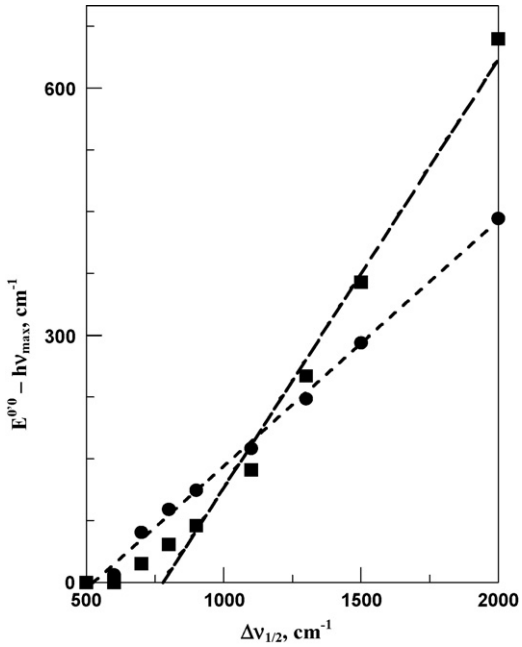

Fig. 4. Shift of the band maxima of emission spectra calculated from rR parameters; squares, $[Ru(bpy)_3]^{2+}$; circles, $[Ru(NH_3)_4bpy]^{2+}$. Least squares lines, respectively: $(E^{0'0} - h\nu_{max}) = (0.52 \pm 0.03)\Delta\nu_{1/2} - (406 \pm 38)$, $r^2 = 0.99$ and $(E^{0'0} - h\nu_{max}) = (0.298 \pm 0.007)\Delta\nu_{1/2} - (157 \pm 9)$, $r^2 = 0.999$.

Even when no molecular distortion coordinates have frequencies smaller than $\Delta\nu_{1/2}$ and when there are no complications arising from the distribution of ground state solvent environments, CT emission bands are expected to be broadened due to the contribution of the solvent reorganizational energy, λ_s [1,2]. Thus, for an experimental emission maximum:

$$h\nu_{max(emis)} \cong E^{0'0} - a\Delta\nu_{1/2} + b - \lambda_s \quad (11)$$

The deconvoluted fundamentals in frozen solution are much better estimates of $E^{0'0}$ than is $h\nu_{max(emis)}$ despite the small contributions from solvent reorganizational energy (most solvent modes will be frozen [8]) and the overlap of vibronic terms; thus, $h\nu_{max(f)}$ may be represented as

$$h\nu_{max(f)} \cong E^{0'0} - \lambda_l \quad (12)$$

where the "effective" low frequency reorganizational, $\lambda_l \cong (\gamma_1 a\Delta\nu_{1/2} + \gamma_2\lambda_s - \gamma_3 b)$ and $\gamma_i \ll 1$. The λ_l contributions are not much of an issue for $h\nu_{max(f)}$ deconvoluted by our procedure, as has been demonstrated by our modeling of the contributions of $\Delta\nu_{1/2}$ to $h\nu_{max(f)}$ [32]. Thus, when the $E^{0'0}$ component makes the strongest contribution to the emission spectrum, and when the highest energy component deconvoluted from the spectrum is carefully matched to the high energy slope, modeling with the rR parameters indicates that $(E^{0'0} - h\nu_{max(f)})/E^{0'0} < 0.001$ for $\Delta\nu_{1/2} \sim 1000\,cm^{-1}$ and $(\Delta\nu_{1/2(fit)} - \Delta\nu_{1/2(actual)})/\Delta\nu_{1/2(actual)} \sim 0.03$–$0.07$ for the $[Ru(L)_4bpy]^{2+}$ complexes [32]. In contrast, this deconvolution procedure overestimates the intensity of the fundamental by 10–15% [32] as a consequence of the overlap with vibronic components.

2.3. Intrinsic bandwidth of the emission

In the limit that $(E_i^{0'0} - \lambda_s)$ does not vary with the solvate and for $h\nu_k > \Delta\nu_{1/2}$ for all distortion modes (k), the bandwidth is expected to be largely a function of temperature and λ_s [1,2]:

$$\Delta\nu_{1/2} \cong 4[k_B T\lambda_s \ln 2]^{1/2} \quad (13)$$

If $(E_i^{0'0} - \lambda_s)$ does vary with the solvate and/or there are some $h\nu_k < \Delta\nu_{1/2}$, $\Delta\nu_{1/2}$ for a CT emission in solution will be larger than this limit. Therefore, the bandwidths inferred from CT emission spectra observed for complexes in solution will generally be larger than the limit expressed in Eq. (13). In view of this consideration and the rR-based modeling described above, we treat $\Delta\nu_{1/2}$ as a parameter characteristic of the experiment, not the molecule or solvent.

2.4. Emission band shapes

The emission intensity on the low energy side of the fundamental contains contributions of vibronic progressions. These vibronic progressions correspond to the projection of the nuclear coordinates of the excited state PE minimum onto the ground state normal coordinates, and each of the distortion modes, k, has a characteristic vibrational frequency, ν_k, and the square of the distortion in each of these modes is represented as a vibrational reorganizational energy, λ_k. This is illustrated for the limit of a single distortion mode in Fig. 5. The amplitude of the displacement of the excited state along the normal coordinate determines the relative intensities of the first and higher order vibronic components of the displacement mode relative to the intensity of the $\{e, 0'\} \rightarrow \{g, 0\}$ transition; e.g., see Fig. 5. The progressions that were used in calculating the spectral curves in Fig. 3 are based on displacement modes inferred from rR spectra, but there are some details and assumptions that are important in the calculations [32]: (a) there are higher order ($j > 1$) as well as

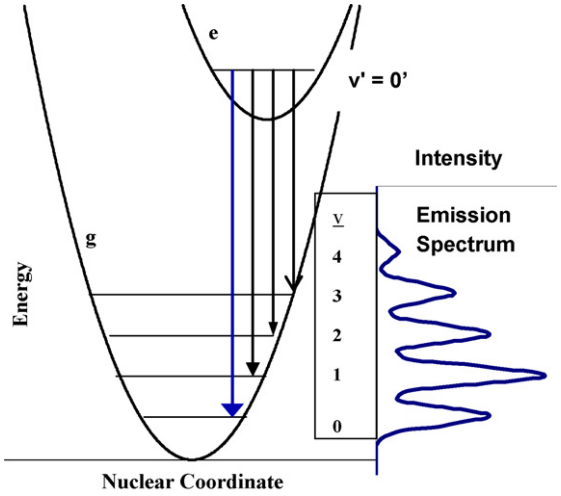

Fig. 5. Illustration of the limit in which the ground and excited state differ in structure by distortion in a single vibrational mode and the bandwidths are very small. The emission spectrum in the inset (right side of the PE curve) was constructed based on a harmonic progression in the distortion mode, Gaussian band shape functions no symmetry restrictions on the coupled modes.

first order ($j = 1$) vibronic contributions to the emission spectrum; (b) the higher order terms used to construct Fig. 3 contain all possible contributions of the displacement modes reported in the rR study; (c) the number of contributing terms increases with the order approximately as n^j and the net contributions of higher order terms can be quite large (e.g., for $n = 10$ displacement modes, there would be approximately 10, 100 and 1000 contributing first, second and third order terms, respectively); (d) the rR data are obtained for vibrations coupled to the spin allowed MLCT absorption, while the emission is nominally for a triplet → singlet transition. The rR parameters used for Fig. 3 fit the observed $[Ru(NH_3)_4bpy]^{2+}$ emission spectra very well; further details related to this fit are described below.

3. Evaluation of the molecular parameters contributing to emission band shapes, and rR-based modeling of observed emission spectra

3.1. Evaluation of the fundamental

3.1.1. Based on the observed spectra

If the emission spectra are of very good quality, with no impurity emissions and very little scattered light, and if the fundamental makes the largest contribution to the emission band envelope, then the fundamental component can be evaluated by matching the slope of the high energy side of the emission to the Gaussian function representing the fundamental [32]. This requires the successive transfer of the digital data files from the fluorimeter to programs such as EXCEL and Gram/32 to obtain the best fit of a Gaussian component representing the emission fundamental, $I_{\nu_{m(f)}}$:

$$I_{\nu_{m(f)}} \cong I_{max(f)}\, e^{-[G_0/w]^2}, \quad G_0 = h\nu_{max(f)} - h\nu_m,$$
$$w = \frac{\Delta\nu_{1/2}}{\sqrt{4 \ln 2}} \tag{14}$$

The parameters, $I_{max(f)}$, $h\nu_{max(f)}$ and $\Delta\nu_{1/2}$, obtained from the observed spectrum are necessary for the subsequent analysis of band shape.

3.1.2. Based on electrochemical measurements

The relationships between CT transition energies and the difference in the potentials for oxidation of the donor and reduction of the acceptor, $F\Delta E_{1/2}$, have been discussed extensively and are reviewed in several places [33,41–43]. Since the electrochemical processes are defined for equilibrium states, they are in principle related to the Δzpe of the two electronic states. However, the electrochemical and optical processes involve different species and: (a) if the excited and ground states differ in spin multiplicity, then there may be substantial contributions of the exchange energies (i.e., for the energy difference between a singlet and triplet state with the same orbital occupation given by $E_{ST} = 2K_{exch}$); (b) the net molecular charge does not change in the optical process, but it changes by one unit in the electrochemical processes; (c) the electrochemical and optical processes involve different changes in orbital occupation. If the last two issues are represented in terms of an electron transfer equilibrium with

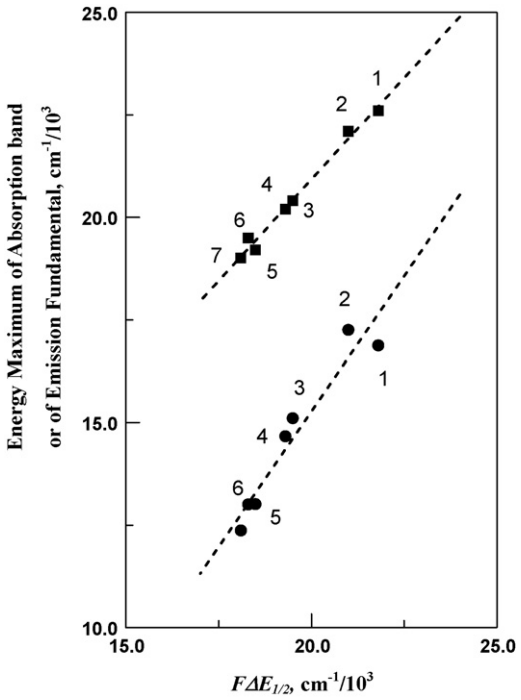

Fig. 6. Correlation of differences between the oxidation and reduction half-wave potentials for $[Ru(L)bpy]^{2+}$ complexes with observed optical transition energies: upper data set for the lowest energy MLCT absorption maximum; lower data set for the energy maximum of the fundamental component deconvoluted from the 77 K emission spectrum. L = $(py)_4$, 1; $(bpy)_2$, 2; (en)bpy, 3; $(NH_3)_2$bpy, 4; $(en)_2$, 5; trien, 6; $(NH_3)_4$, 7. The least squares lines are calculated for the data points 1–7: slope = 0.99 ± 0.05 and intercept = 1 ± 1, top; 1.3 ± 0.2 and −11 ± 3, bottom.

equilibrium constant K_{DA} [33,44]:

$$\{D^+,A\} + \{D,A^-\} \overset{K_{DA}}{\rightleftarrows} \{D^+, A^-\} + \{D,A\} \tag{15}$$

then for a singlet–singlet transition [33,42–44] under ambient conditions:

$$E^{00'} \cong -F\Delta E_{1/2} - RT \ln K_{DA} + T\Delta S^\circ$$
$$\cong -F\Delta E_{1/2} - RT \ln K_{elec} + 2\alpha_{ge}\lambda_s + T\Delta S^\circ \tag{16}$$

where K_{elec} is a purely electrostatic contribution. For a triplet–singlet transition [32,44]:

$$E^{0'0} \cong -F\Delta E_{1/2} - RT \ln K_{elec} + 2\alpha_{eg}\lambda_l + T\Delta S^{\circ\prime} - 2K_{exch} \tag{17}$$

For reasons described above, the fundamental component in the broad and structureless ambient absorptions of the $[Ru(L)_4bpy]^{2+}$ complexes are generally difficult to uniquely identify; therefore, we have used the absorption maxima, $h\nu_{max(abs)}$, for the correlations in Fig. 6; it is important to note that the common assumption that $h\nu_{max(abs)} \cong E^{00'} + \lambda_s$ is not generally correct; see the discussion above. Clearly the absorption maxima agree with Eq. (16) (slope = 0.99 ± 0.05; intercept = 1000 ± 1000 cm^{-1}). While the values found for $h\nu_{max(f)}$ in 77 K solutions also correlate with $F\Delta E_{1/2}$, the slope is steeper than expected (1.3 ± 0.2) and the intercept is very negative (−11,000 ± 3000 cm^{-1}); these features probably arise mostly

from systematic variations in the contributions of $2K_{exch}$ in Eq. (17) since the exchange energies have been calculated to be of the order of a few thousand wavenumbers for these complexes and to be much larger for $[Ru(NH_3)_4bpy]^{2+}$ than for $[Ru(bpy)_3]^{2+}$ [45].

3.2. The basis for evaluating the relative intensity contributions of the distortion modes

Eq. (6) represents the vibronic contributions as a series of j^{th} order polynomials (in S_1) with Gaussian shape functions centered at the energy of the vibrational quantum. It is convenient to collect terms according to the order of the polynomials so that for $S_t \ll 1$ the first, second and third order vibronic contributions are, respectively:

$$I_{\nu_m(0'1)} \cong I_{max(f)} \sum_i \left(\frac{\lambda_i}{h\nu_i}\right) e^{-[G_i/w]^2},$$

$$G_i = h\nu_{max(f)} - h\nu_i - h\nu_m \quad (18)$$

$$I_{\nu_m(0'2)} \cong \frac{I_{max(f)}}{2} \sum_i \sum_j \left(\frac{\lambda_i}{h\nu_i}\right)\left(\frac{\lambda_j}{h\nu_j}\right) e^{-[G_{ij}/w]^2},$$

$$G_{ij} = h\nu_{max(f)} - h\nu_i - h\nu_j - h\nu_m \quad (19)$$

and

$$I_{\nu_m(0'3)} \cong \frac{I_{max(f)}}{6} \sum_i \sum_j \sum_k \left(\frac{\lambda_i}{h\nu_i}\right)\left(\frac{\lambda_j}{h\nu_j}\right)\left(\frac{\lambda_k}{h\nu_k}\right) e^{-[G_{ijk}/w]^2},$$

$$G_{ijk} = h\nu_{max(f)} - h\nu_i - h\nu_j - h\nu_k - h\nu_m \quad (20)$$

We have used Eqs. (18)–(20) and the rR parameters reported for $[Ru(bpy)_3]^{2+}$ [46] and $[Ru(NH_3)_4bpy]^{2+}$ [40] to model the respective emission spectra, Fig. 7, and to evaluate the procedures used in the band shape analyses described here [32]. The spectral fits are excellent for $[Ru(NH_3)_4bpy]^{2+}$ and reasonable for $[Ru(bpy)_3]^{2+}$.

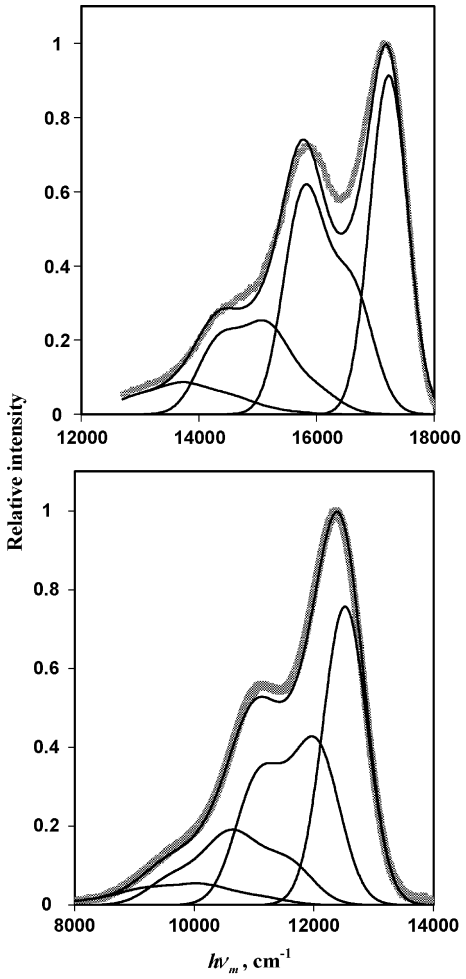

Fig. 7. Fits of resonance-Raman data to the 77 K emission spectra of $[Ru(bpy)_3]^{2+}$ in DMSO/water, top, and $[Ru(NH_3)_4bpy]^{2+}$ in butyronitrile, bottom. The heavy gray lines are the experimental spectra; the curves of lower intensity, from right to left, are: the fundamental; the sum of first order vibronic components; the sum of second order vibronic components; the sum of third order vibronic components. The sum of all these components is the thin black line that is nearly coincident with the experimental spectrum. Taken from Fig. 4 in [32].

3.3. Variations in vibrational reorganizational energies: reorganizational energy profiles (emreps) [32]

3.3.1. The basis for constructing emreps from the observed spectra

As outlined in the preceding section, the emission band shape is determined by the contributions of progressions in the distortion modes, each making an intensity contribution of the type:

$$(I_{\nu_m(0'j)})_k \cong \left[\frac{1}{j!}\left(\frac{\lambda_k}{h\nu_k}\right)^j e^{-[G_{jk}/w]^2}\right] I_{\nu_m(f)} \quad (21)$$

Because the λ_k contain the information about excited state structure they are key parameters in determining excited state lifetimes and electron transfer reactivity it is convenient to reconfigure the vibronic contributions to the emission band shape so as to emphasize the vibrational reorganizational energy contributions. A simple means for doing this is based on the maxima of the first order intensity contributions to the emission spectrum, Eq. (18) and [47,48]:

$$\lambda_k = \left(\frac{I_{max(k)}}{I_{max(f)}}\right) h\nu_k \quad (22)$$

In order to accomplish this, the contribution of the fundamental component, corresponding to the $\{e, 0'\} \rightarrow \{g, 0\}$ transition, is removed from the experimental spectrum to generate a difference spectrum, $I_{\nu_m(diff)} = I_{\nu_m(expt)} - I_{\nu_m(f)}$, and a profile of the reorganizational energy contributions is generated by multiplying the normalized difference spectrum, $I_{\nu_m(diff)}/I_{max(f)}$, by the spectral frequency difference from the fundamental, $h\nu_d = h[\nu_{max(f)} - \nu_m]$. Constructed in this manner, the reorganizational energy profile will have maxima at vibrational energies different from those of the normal vibrational modes because the functions generated are of the form $\Lambda_k = h\nu_k e^{-[G_{jk}/w]^2}$ and not Gaussian. An approximate cor-

rection for this effect is based on first order terms [32] with $h\nu_x \cong 2(h\nu_d) - [(h\nu_d)^2 + (\Delta\nu_{1/2})^2/4\ln 2]^{1/2}$; thus, the first, second and third order functions that contribute to the reorganizational energy profile and correspond to the respective vibronic contributions are

$$\xi_I = h\nu_x \sum_i \left[\left(\frac{\lambda_i}{h\nu_i} \right) e^{-[G_i/w]^2} \right] \quad (23)$$

$$\xi_{ij} = h\nu_x \frac{1}{2} \sum_i \sum_j \left[\left(\frac{\lambda_i}{h\nu_i} \right) \left(\frac{\lambda_j}{h\nu_j} \right) e^{-[G_{ij}/w]^2} \right] \quad (24)$$

$$\xi_{ijk} = h\nu_x \frac{1}{6} \sum_i \sum_j \sum_k \left[\left(\frac{\lambda_i}{h\nu_i} \right) \left(\frac{\lambda_j}{h\nu_j} \right) \left(\frac{\lambda_k}{h\nu_k} \right) e^{-[G_{ijk}/w]^2} \right] \quad (25)$$

The empirical reorganizational energy profile (emrep) generated from the emission spectrum is then

$$\Lambda_x = h\nu_x \frac{I_{\nu_m(\mathrm{diff})}}{I_{\nu_{\max(f)}}} = \xi_i + \xi_{ij} + \xi_{ijk} + \cdots \quad (26)$$

3.3.2. Uses and significance of emreps

While the emreps are composite quantities when based on solution spectra, they map into the vibrational reorganizational energies for $\Delta\nu_{1/2} \ll 100\,\mathrm{cm}^{-1}$ [32]. Furthermore, they provide a systematic means for examining excited state structural variations in related series of complexes and they facilitate the identification of the contributions of the highest frequency vibrational modes, such as the N–H or C–H stretching modes, whose contributions to the emission spectrum are small owing to their large values of $h\nu_i$. While these vibrational modes are expected to dominate excited state relaxation pathways [16,17,19], but rR studies have not been able to establish limits on their contributions to excited state distortions in most of the complexes of interest, in part because their frequencies are so large. Such limits have been established by using emreps [32,49,50].

3.4. Other considerations

3.4.1. Selection rule issues

In general, the vibrationally equilibrated CT excited states will have lower symmetry than the corresponding ground states, and we have assumed in studies summarized below that all of the vibrational modes that are resolved in rR studies also contribute to the emission band shape and that there are no symmetry constraints on the contributions of vibrational fundamentals, harmonics or combinations. This contrasts to the ^{2}E ligand field (LF) excited state of Cr^{III} which usually differs little from the geometry of the ground state, and for which selection rules are very important in determining the relative importance of component contributions to the emission spectrum as discussed elsewhere [51–54]; e.g., see Fig. 2.

3.4.2. Experimental artifacts

Some contributions to the band shape can arise from the techniques used in emission spectral data collection. The principal concerns are: (a) spectrometer response; (b) sample quality; (c) scattered light. It is necessary to calibrate the spectrometer response against reliable wavelength and intensity standards, and there are several available options [36]. The principal sample quality issues in 77 K glasses are: (i) emitting impurities; (ii) glass quality; (iii) particles in the light path (e.g., dust or condensation on the sample cell); (iv) other sources of scattered light. Obviously, impurities must be eliminated, but it may be less obvious that a fractured or otherwise poor quality glass results in a distorted band shape. Such effects are a consequence of a combination of the increases light scattering, which results in poor wavelength discrimination, and the increased multiplicity of environments of the emitting species.

4. Effects of configurational mixing

4.1. General

Transition metal complexes typically have several electronic states with energies that are relatively close to that of the emitting state, and these energy differences and the resulting configurational mixing can vary systematically through a series of related complexes. The effect of configurational mixing of two electronic states ("1" and "2") is to reduce the extent to which they differ. It is convenient to treat this effect in terms of Eq. (4) [4]. Thus, the extent of configurational mixing depends on $\alpha_{12} = H_{12}/E_{12(d)}$, where H_{12} is the normalized electronic matrix element $E_{12(d)}$ is the vertical energy difference between the unmixed (or diabatic) electronic states.

4.2. Excited state–ground state mixing

4.2.1. Transition energies

The qualitative effects of configurational mixing between electronic states (note that any exchange energy contributions will be contained in $E_{12}^{0'0}$) are: (a) to increase $E_{12(d)}$ when $E_{12}^{0'0} > 0$; (b) to move the potential energy (PE) minima of the two states closer together (i.e., to reduce the excited state distortion), see Fig. 8. When the vibrational modes of the unmixed ground and electronic excited states have the same vibrational frequencies (or force constants) and there is very little distortion ($\alpha_{ij}^2 \ll 0.1$), configurational mixing results in [4,33]:

$$E_{12} = E_{12}^{0'0} + \lambda_r \cong E_{12(d)}(1 + 2\alpha_{12}^2) - 2\lambda_{r(d)}(\alpha_{12}^2 + \alpha_{21}^2 + \cdots) + \delta\Delta\mathrm{zpe} \quad (27)$$

where $\lambda_{r(d)}$ is the effective (diabatic) reorganizational energy and the next to last term in Eq. (25) is a result of the shift of the PE minima and the last term is only important if there are differences in the ground and excited state force constants [50].

4.2.2. Effect on force constants and vibrational frequencies

When there is appreciable configurational mixing between electronic states, the shapes of the PE surfaces are altered, as indicated in Fig. 8, and this implies that when α_{ij}^2 is sufficiently large, the force constants will also be altered. This will result in

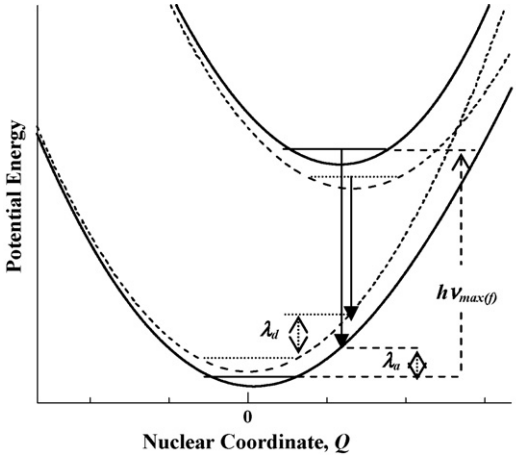

Fig. 8. Potential energy curves qualitatively illustrating the effects of configurational mixing on the reorganizational energy, λ (a for adiabatic and d for diabatic): $\lambda_a < \lambda_d$.

a change of the zpes of the mixed electronic states and thus will modify the transition energy. This can be expressed in terms of changes in the force constants; the force constant, f_k, of a vibrational mode k is given by the second derivative of the PE with respect to the correlated normal coordinate, Q_k:

$$f_k = \frac{\partial^2(\mathrm{PE})}{\partial Q_k^2} \tag{28}$$

In general, configurational mixing alters the force constants in two different ways [50]: (a) any difference in the force constants (and vibrational frequencies) of the two electronic states is decreased; (b) the force constants (and vibrational frequencies) of the higher energy electronic state are increased while the force constants (and vibrational frequencies) for the lower energy state are decreased (a result of the change of shape of the PE surfaces). While this is a minor issue in regard to Δzpes and it may implicate configurational mixing among CT excited states [50], it is not an important factor in the analysis of emission band shapes and it will not be further considered here.

4.2.3. Vibronic sideband intensities

Since configurational mixing reduces the excited state distortion, represented in Fig. 8 by the reduced separation of PE minima along the effective nuclear distortion coordinate, the effective reorganizational energy is also reduced [33,44,55–57]; if we allow for weaker electronic coupling when the two states differ in spin multiplicity (i.e., $\alpha_{ge}^2 > \alpha_{eg}^2$ and a smaller shift of the excited state than of the ground state PE minimum), then for $\alpha_{ge}^2 < 0.1$ the shifts of the PE minima along any distortion coordinate result in

$$\lambda_k \cong \lambda_{k(d)}(1 - 2\alpha_{ge}^2 - 2\alpha_{eg}^2) \tag{30}$$

The individual vibronic components are not resolved in a broad band spectrum, but the average attenuation of the vibronic components will appear as changes in intensity of the emreps (at least in a two state limit) and Eq. (30) may be rewritten as

$$\Lambda_r \cong \Lambda_{r(d)}(1 - 2\alpha_{ge}^2 - 2\alpha_{eg}^2) \tag{31}$$

For example, the emitting Ru/bpy MLCT excited states have been found with energies of 12,000–18,000 cm^{-1}, so that configurational mixing of the MLCT excited states with their ground electronic states is expected to result in smaller differences molecular structures of these states as the excited state energy decreases. Furthermore, the electronic matrix elements, H_{ge}, found for mixing the singlet ground states with the singlet MLCT excited states in Ru–polypyridyl complexes are very large [44,58] and H_{ge} has been estimated to be about 7000 cm^{-1} for Ru/bpy complexes [44]; even the matrix element for the ^{3}MLCT/ground state mixing, H_{eg}, appears to be large in Ru/polypyridyl complexes ($H_{eg} > \sim H_{ge}/3$) [58], probably as a result of spin–orbit coupling and $H_{eg} \approx (H_{SO}/2K_{exch})H_{ge}$ (where H_{SO} is the matrix element for mixing the singlet and triplet MLCT excited states with the same electronic configurations). In view of this, Eq. (31) indicates that the differences in the excited state configurational mixings will be manifested in the emission spectra by substantial differences in the vibronic sideband intensities, and such differences have been observed [59]. The energy differences between electronic excited states may also vary through a series of complexes and such variation can result in important differences in the structures and properties of the lowest energy excited states, but this is more difficult to directly examine experimentally since the higher energy excited states are difficult to observe and characterize.

4.3. Band shape variations implicating configurational mixing among excited states

While the band shape of an emission spectrum is related to the structural differences between the lowest energy excited state, $\{e_0\}$, and the ground state, transition metal complexes characteristically have several other excited states whose energies differ little from that of $\{e_0\}$ [44,57,60,61]; e.g., see Fig. 9. The general effects of this ground state–excited state configurational mixing on the energies and vibrational reorganizational energies of $\{e_0\}$ follow the patterns described above. Fig. 9 suggests that configurational mixing with higher energy metal-centered (ligand field, LF) and ligand-centered ($\pi\pi^*$) excited states should be considered for these complexes.

4.3.1. Possible ^{3}MLCT mixing ^{3}LF excited states

Although there is no direct experimental information about the LF excited states of $[Ru(L)_4bpy]^{2+}$ complexes, such states have often been implicated in the ambient ^{3}MLCT decay and photochemistry of these complexes [62–65] and such a thermally activated reaction or decay pathway would be possible only if the energy differences are small relative to about $17k_BT$ or $<9k_BT$ for $[Ru(bpy)_3]^{2+}$ and $[Ru(NH_3)_4bpy]^{2+}$, respectively, for ambient conditions. An estimate of the of a ^{3}LF excited state can be based on comparison to $[M(NH_3)_6]^{n+}$ analogs. Thus, $[Rh(NH_3)_6]^{3+}$, which is isoelectronic with $[Ru(NH_3)_6]^{2+}$, has a broad ^{3}LF ($^3T_{1g}$) emission band centered at about 17,000 cm^{-1} with an origin at about 21,000 cm^{-1} [66]. This band is attributed to vibronic progressions in the $a_{1g}(O_h)$ ($\nu_{a_{1g}} = 500\,cm^{-1}$) and $e_g(O_h)$ ($\nu_{e_g} = 480\,cm^{-1}$) Rh–N skeletal vibrational modes in

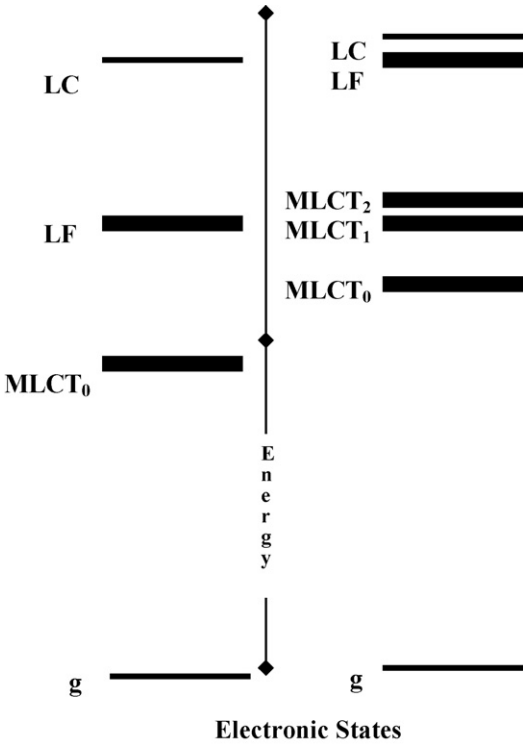

Fig. 9. Energy diagram qualitatively illustrating the electronic states for complexes with one (left) and three (right) nominally degenerate MLCT excited states. A localized model of C_2 or C_{2v} symmetry is assumed; e.g., most electron density localized on a single bpy of $[Ru(bpy)_3]^{2+}$ for the scheme at the right. The energy differences are presumed to be relative to the ground state nuclear coordinates. The heavy bars indicate that several combinations of metal-centered orbitals can contribute to the excited state electronic configurations. The relative energies of the electronic states are estimated based on spectra reported for $[Ru(L)bpy]^{2+}$ or for closely related complexes [44,45,53,57,60,61]; only the MLCT excited states involving bpy LUMO are considered for simplicity. For these complexes the vertical bar corresponds to an energy range of about 40,000 cm^{-1} LF = ligand field (dd) excited state; LC = ligand-centered excited state (e.g., $\pi\pi^*$).

which the excited state is so distorted that the Huang–Rhys parameter is estimated to be $S_{a_{1g}} \cong 0.6$ and $S_{e_g} \cong 14$, respectively [66]. The latter is nearly 50 times larger than the largest value of S_k inferred from rR spectra of either $[Ru(bpy)_3]^{2+}$ [46] or $[Ru(NH_3)_4bpy]^{2+}$ [40]. The lower charge results in lower energy LF excited states in $[Ru(NH_3)_6]^{2+}$ than in $[Rh(NH_3)_6]^{3+}$, with the lowest energy LF absorption maxima at about 26,500 and 32,500 cm^{-1}, respectively [60,66]. If there is a similar energy difference for the ^{3}LF excited states (note that this assumes similar exchange energies, so that there is considerable uncertainty in the estimate), then the ^{3}LF state of $[Ru(NH_3)_6]^{2+}$ should have its origin in the 15,000–17,000 cm^{-1} energy range. The energies of the LF states can be represented by the electronic pairing energy and the energy differences of the dσ and dπ orbitals, or $10Dq \cong 3\sigma_L - 4\pi_L$, where σ_L and π_L are the respective orbital energy parameters of the angular overlap model (AOM) [60,67,68]. The σ_L-parameters are typically the same for the am(m)ine and pyridyl ligands, but the π_L-parameters, usually taken as zero for am(m)ines, are found to be significantly negative for pyridyl ligands [67,68]. Thus, $\pi_L \cong -250\ cm^{-1}$ [69] (per N) has been found for $[Cr(bpy)_3]^{3+}$, and the π_L-parameter for $[Ru(bpy)_3]^{2+}$ are probably more negative. These considerations indicate that the ^{3}LF state energies are only a few thousand wavenumbers larger than the ^{3}MLCT energies, and they could approximately track the variations of ^{3}MLCT energies in the $[Ru(Am)_{6-2n}(bpy)_n]^{2+}$ complexes. The tetragonally distorted $^3T_{1g}$ excited state of the octahedral complexes [66], will be split into two or more components in the low symmetry $[Ru(L)_4bpy]^{2+}$ complexes and each of these components will be distorted with respect to the ground state metal–ligand normal coordinates. Configurational mixing between the ^{3}MLCT and the highly distorted ^{3}LF excited states will tend to increase some distortion coordinates of the lowest energy excited state. Since the ^{3}LF excited state has a dσ dπ electronic configuration and the ^{3}MLCT state has a dπ pπ electronic configuration, the electronic coupling matrix element, $H_{CT,LF}$, could be small as a result of the small values of the corresponding overlap integrals [4]. If this is the case, then the mixing coefficients, $\alpha_{CT,LF}$, will be significant only for small values of the differences in energies between these states.

4.3.2. Possible mixing between different MLCT excited states

When more than one polypyridyl ligand is coordinated to a metal or in complexes with more than one metal, configurational mixing between the different (diabatic) MLCT excited states should also be considered. Such configurational mixing has the effect of reducing the electron density localized on any one ligand in the excited state and has the formal effect of adding $[2(\alpha_{ge}^2 \Lambda_{r(d)} - 2\alpha_{01}^2 \Lambda_{l(d)})]$ to Eq. (31), where α_{01} is the MLCT/MLCT′ mixing coefficient and $\Lambda_{l(d)}$ is a reorganizational energy parameter for MLCT → MLCT′ electron transfer [70]. If the effective force constants are the same in all states, then $\Lambda_{r(d)} = \Lambda_{l(d)}$.

For example consider the $[Ru(L)_2(bpy)_2]^{2+}$ complexes in which the two MLCT excited states form a mixed valence pair:

$$[(bpy)\text{–}\{Ru^{III}(L)_2\}\text{–}(bpy^-)]^{2+} \rightleftarrows [(bpy^-)\text{–}\{Ru^{III}(L)_2\}\text{–}(bpy)]^{2+} \quad (32)$$

A variety of experimental evidence suggests that there is little configurational mixing between degenerate ^{3}MLCT excited states with different electronic configurations such as are illustrated in Eq. (32) [50,71,72]; evidence for a contrasting view has also been presented [73,74]. Weak coupling between the degenerate electronic configurations is consistent with a superexchange mechanism for the electronic coupling in which electronic coupling is mediated by an excited state in which the electron has been transferred to the bridging moiety (in this case Ru^{III}) [11,75,76]. The mediating higher energy excited state for mixing ^{3}MLCT$_0$ and ^{3}MLCT$_1$ (notation as in Fig. 9), would be a triplet ^{3}LF excited state. Therefore, the superexchange coupling matrix element can be formulated as [11,76]:

$$H_{01}^{spx} \approx \frac{H_{CT,LF}^2}{E_{CT,LF}} \approx \alpha_{CT,LF}^2 E_{CT,LF} \quad (33)$$

$E_{CT,LF}$ is the sum of the difference in zpe between these states and a very large reorganizational energy term (roughly the sum of the vibrational reorganizational energies for the $[Ru(bpy)_3]^{2+}$ ^{3}MLCT and ^{3}LF excited states, which is possibly greater than 5000 cm^{-1}), and $H_{CT,LF}$ may be relatively small as a result of poor orbital overlap (see discussion above). Consequently, $\alpha^2_{CT,LT}$ and H^{spx}_{01} are expected to be very small leading to very little mixing of the ^{3}MLCT excited states.

Configurational mixing between CT and "local" excited states (LC for these complexes) has been postulated as a source of the intensity of CT transitions [4]. We have not found any variations in band shapes that clearly implicate different contributions of the mixing with LC states.

5. Applications to the 77 K emission spectra of $[Ru(L)_4bpy]^{2+}$ complexes

The well known and well characterized $[Ru(L)_4bpy]^{2+}$ systems have been used as substrates with respect to which the approaches described here can be tested and to examine the extent to which these approaches can yield new information about the excited states of these complexes [32]. The rR parameters reported for $[Ru(bpy)_3]^{2+}$ [46] and $[Ru(NH_3)_4bpy]^{2+}$ [40] fit the observed emission spectra well based on Eqs. (14)–(16), and they have been used to model the approaches described above, and to estimate the bandwidth dependent uncertainties in the parameters that are extracted from analysis of emission band shapes [32]. The rR-based modeling is discussed in detail elsewhere [32], and in this section we will summarize some of the excited state properties that have been inferred from systematic comparisons of the MLCT emission band shapes.

5.1. Pertinent rR observations

Table 1 summarizes the rR parameters found for several metal–bipyridine complexes, and their maximum first order intensity contributions (relative to $I_{max(f)} = 1$) to the emission spectrum; see Eqs. (14) and (18). The comparison of the Huang–Rhys factors for these complexes in Fig. 10 suggests that the rR active vibrations at 1490 and 1560 cm^{-1} arise almost entirely from distortions of the bpy ring in the MLCT excited states of $[Ru(L)_4bpy]^{2+}$ complexes ($S_k = 0.13 \pm 0.01$ and 0.28 ± 0.02, respectively); peaks at 1320 and 1600 cm^{-1} may also be characteristic of the bpy distortions, but there seems to be more variability with $(L)_4$. The similar displacements found at 1490 and 1560 cm^{-1} for $[Ru(bpy)_3]^{2+}$ [46], $[Os(bpy)_3]^{2+}$ [26] and $[Os(py)_4bpy]^{2+}$ [26] are surprising. The smaller values of S_k at these frequencies for $[Ru(NH_3)_4bpy]^{2+}$, $S_k([Ru(NH_3)_4bpy]^{2+}) = 0.57 S_k(L')$ for Ru with $(L')_4 = (bpy)_2$ is readily attributed to the attenuation predicted by Eq. (30) since $h\nu_{max(abs)}$ and $h\nu_{max(f)}$ are smaller for $[Ru(NH_3)_4bpy]^{2+}$ than for $[Ru(bpy)_3]^{2+}$, resulting in greater sideband attenuation (larger α^2_{ij}) for the former [32].

In contrast, the distortions in the lower frequency vibrational modes ($h\nu_k < 700$ cm^{-1}) depend strongly on

Table 1
Comparison of resonance Raman parameters

$[Ru(bpy)_3]^{2+}$ [a]			$[Os(bpy)_3]^{2+}$ [b]			$[Ru(NH_3)_4bpy]^{2+}$ [c]			$[Os(py)_4bpy]^{2+}$ [b]			$[Os(py)_2(bpy)_2]^{2+}$ [b]		
ν_k (cm^{-1})	S_k	λ_k (cm^{-1})	ν_k (cm^{-1})	S_k	λ_k (cm^{-1})	ν_k (cm^{-1})	S_k	λ_k (cm^{-1})	ν_k (cm^{-1})	S_k	λ_k (cm^{-1})	ν_k (cm^{-1})	S_k	λ_k (cm^{-1})
1608	0.048	77	1606	0.063	101	1605	0.072	116	1606	0.080 (0.070)	128 (112)	1606	0.060 (0.060)	96 (96)
1563	0.110	172	1558	0.125	195	1548	0.065	101	1558	0.140	218	1558	0.128	199
1491	0.266	397	1485	0.266	395	1481	0.151	224	1485	0.225	334	1485	0.273	405
1320	0.157	207	1323	0.073	97	1331	0.084	112	1323	0.070	93	1323	0.071	94
1276	0.065	83												
1264	0.004	5	1265	0.049	62	1260	0.011	14	1265	0.025	32	1265	0.041	52
									1218	(0.090)	(110)	1218	(0.012)	(15)
1176	0.115	135	1174	0.062	73	1172	0.045	53	1174	0.045	53	1174	0.065	76
1110	0.013	14	1108	0.002	2				1108	0.004	4			
1067	0.003	3							1066	0.006	6	1066	0.002	2
1043	0.013	14	1049	0.004	4	1027	0.051	52	1053	0.004	4	1036	0.009	9
			1030	0.028	29				1030	0.020	2	1025	0.015	15
			1015	0.010	10				1015	0.015 (0.008)	2	1011	0.015 (0.008)	15 (8)
									1006	0.021 (0.015)	2			
766	0.10	77												
668	0.281	188	669	0.019	13	667	0.192	127	666	0.018	12	670	0.017	11
						456	0.036	16						
370	0.10	37	375	0.014	5	376	0.328	123	375	0.016	6	375	0.018	7
283	0.125	35				248	0.106	26	280	0.012	3	280	0.005	1

[a] [46].
[b] [26].
[c] [40].

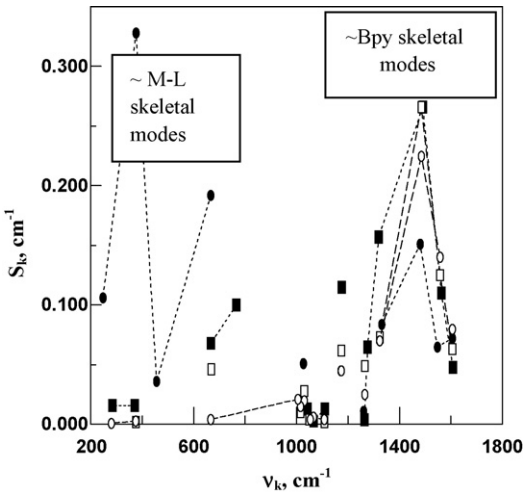

Fig. 10. Comparison of rR Huang–Rhys factors for simple M-bpy complexes: $[Ru(bpy)_3]^{2+}$ [46], filled rectangles; $[Os(bpy)_3]^{2+}$ [26], open rectangles; $[Ru(NH_3)_4bpy]^{2+}$ [40], filled circles; $[Os(py)_4bpy]^{2+}$ [26], open circles. Dashed lines are drawn connecting some of the data points for each complex to simplify comparisons.

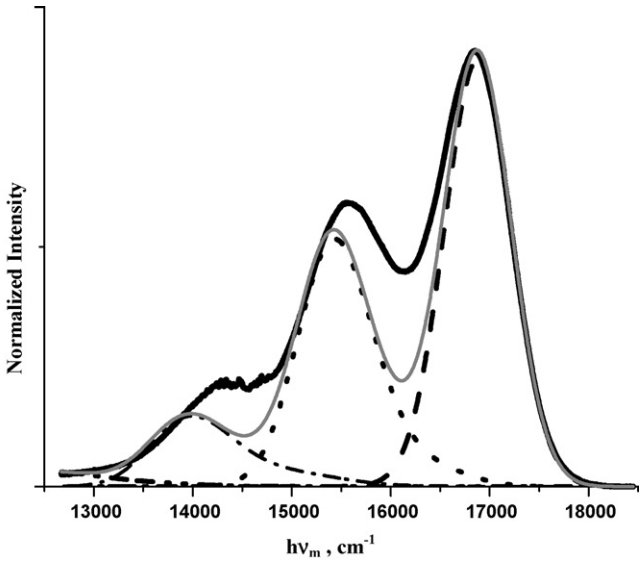

Fig. 11. The emission spectrum of $[Ru(py)_4bpy]^{2+}$ in butyronitrile at 77 K compared to that calculated from the rR parameters reported for $[Os(py)_4bpy]^{2+}$ [26]; see Table 1. For the observed spectum solid black curve with $h\nu_{max(f)} = 16{,}880\,cm^{-1}$ and $\Delta\nu_{1/2} = 800\,cm^{-1}$. Fundamental, $I_{(f)}$, long-dash curve; sum of first order components, short-dash curve; sum of second order components, dash-dot curve; sum of third order components, dash-dot-dot curve; sum of all components, solid gray curve.

L and on the metal, and they decrease in the order $[Ru(NH_3)_4bpy]^{2+} \gg [Ru(bpy)_3]^{2+} > [Os(L)_4bpy]^{2+}$. These can be assigned as largely metal–ligand skeletal modes [40,77]. The large amplitude of these vibrations for $[Ru(NH_3)_4bpy]^{2+}$ indicates that there is a large difference in the ground and excited state coordination sphere bond lengths and angles of this complex, nominally between the Ru(II) and Ru(III) oxidation states. This can be compared to the Ru(II)–N and Ru(III)–N bond length differences of $[Ru(NH_3)_6]^{3+/2+}$ and $[Ru(bpy)_3]^{2+}$ which are 4 pm and probably less than 1 pm [78], respectively. This corresponds to a coordination sphere reorganizational energy, including all skeletal vibrational modes, of about 240 and $\sim 0\,cm^{-1}$, respectively [14]; by interpolation the coordination sphere reorganizational energy of $[Ru(NH_3)_4bpy]^{2+}$ should be about $160\,cm^{-1}$. However, the sums of all rR reorganizational energies reported for the vibrational modes with $h\nu_k < 700\,cm^{-1}$ in these two complexes are 294 and $260\,cm^{-1}$ (see Table 1), respectively. Thus, the coordination sphere distortions for both of these complexes appear to be larger than expected based on known ground state electron transfer behavior: if one assumes that the attenuation described by Eq. (27) applies equally to coordination sphere and to bpy distortions in the MLCT excited states, then the vibrational reorganizational energies for the coordination sphere displacement modes in the $[Ru(NH_3)_4bpy]^{2+}$ MLCT excited state are about $200\,cm^{-1}$ larger than expected for a simple two state electron transfer process. A possible origin of this discrepancy is configurational mixing between the ^{3}MLCT excited state and a slightly higher energy ligand field excited state (^{3}LF). Furthermore, the rR parameters reported for $[Os(py)_4bpy]^{2+}$ [26] do not account for the intensity of the $[Ru(py)_4bpy]^{2+}$ emission spectrum in the frequency regime of the low frequency distortion modes, Fig. 11. That there is so much variation in the contributions of low frequency distortion modes to the band shapes of these complexes is reasonably consistent with different extents of configurational mixing with a low energy ^{3}LF excited state. However, there is no direct information about the energy variations of these states among these complexes, and other explanations for the observed variations should also be considered. For example, the discrepancies between the emission spectrum of $[Ru(bpy)_3]^{2+}$ calculated using rR parameters and that observed may arise from differences in the symmetry of the Franck–Condon excited state that is probed by the rR experiment and the emitting state, since the former must have the D_3 ground state symmetry while the latter could have C_2 symmetry if the excited electron is largely localized in a single bpy ring [32].

5.2. *Vibronic attenuation in frozen solutions and the evaluation of the extent of configurational mixing*

Because the bpy modes in the $h\nu_k = 1500\,cm^{-1}$ region have the largest vibrational reorganizational energies (for the vibrations at about $1490\,cm^{-1}$ $\lambda_k = 397$ and $224\,cm^{-1}$, respectively for $[Ru(bpy)_3]^{2+}$ and $[Ru(NH_3)_4bpy]^{2+}$; see Table 1), and because the rR data seem to indicate that these modes are mostly bpy-centered vibrations, the corresponding emrep amplitudes may be relatively good probes of the overall properties of the MLCT excited states in polypyridyl complexes.

The fits between the observed and calculated (based on rR parameters and Eqs. (14)–(16)) 77 K emission spectra of $[Ru(NH_3)_4bpy]^{2+}$and $[Ru(bpy)_3]^{2+}$ [32] are shown in Fig. 7. An important observation is that the second and third order vibronic terms, based on the rR parameters and Eqs. (15) and (16), contribute significantly to the band shape, as shown

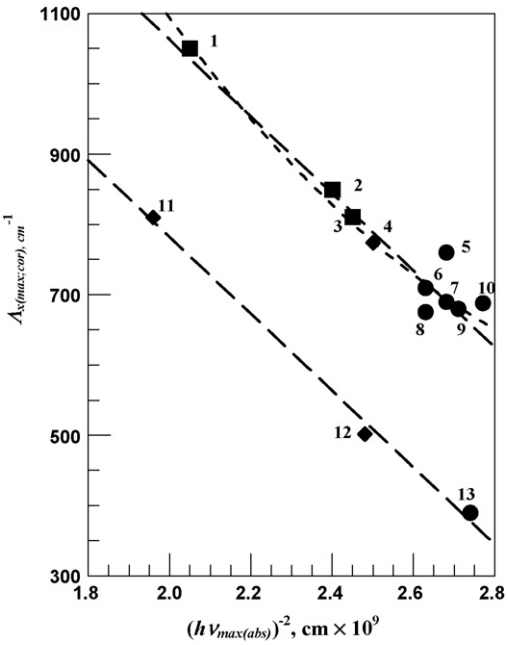

Fig. 12. The variation of emrep amplitudes (corrected for bandwidth differences), $\Lambda_{x(max;cor)}$, with $(h\nu_{max(abs)})^{-2}$ for $[Ru(L)bpy]^{2+}$ complexes with L = $(bpy)_2$, 1; en(bpy), 2; $(NH_3)_2$(bpy), 3; $(Me_2pyo[14]eneN_4)$, 4; (*rac*-$Me_6[14]aneN_4$), 5; ($[14]aneN_4$), 6; ($[15]aneN_4$), 7; trien 8; $(en)_2$, 9; $(NH_3)_4$, 10; $(py)_4$, 11; ($[12]eneN_4$), 12; ($[12]aneN_4$), 13, from [79]. The best fit curves for the top set of data points are (large dashes): $\Lambda_{x(max;cor)} = 2200 \pm 100 - (550 \pm 40) \times 10^9\ (h\nu_{max(abs)})^{-2}$ and (small dashes): $\Lambda_{x(max;cor)} = 3800 \pm 900 - (1900 \pm 700) \times 10^9\ (h\nu_{max(abs)})^{-2} + (280 \pm 150) \times 10^{18}\ (h\nu_{max(abs)})^{-4}$. For the lower data set: $\Lambda_{x(max;cor)} = 1900 \pm 100 - (550 \pm 40) \times 10^9\ (h\nu_{max(abs)})^{-2}$.

in Fig. 7. The fits of rR parameters to the emission spectra are quite good, especially for $[Ru(NH_3)_4bpy]^{2+}$, considering that rR parameters were obtained from excitation of the ^{1}MLCT absorption bands in ambient solutions. For example, since the $^1\{g\} \rightarrow {}^1$MLCT absorption is allowed while the ^{3}MLCT $\rightarrow {}^1\{g\}$ emission is expected to be at least partly forbidden, one might expect less attenuation of the emission, for which $H_{eg}(^3\text{MLCT}) < H_{ge}(^1\{g\})$ in Eq. (31), than for the absorption for which $H_{eg}(^1\text{MLCT}) = H_{ge}(^1\{g\})$; however, this may be partly compensated by the energy differences between the PE minima of the two states ($E_{ST} \cong 2K_{exch}$).

The vibronic sideband contributions to the observed emission spectrum are nearly 40% smaller for $[Ru(NH_3)_4bpy]^{2+}$ than for $[Ru(bpy)_3]^{2+}$ [32,59]; see Fig. 7. The similar contrast in the sideband contributions in the calculated spectrum reflect the contrasts in the bpy distortion modes noted in Section 5.1 above. Through the simple series of $[Ru(Am)_{6-2n}(bpy)_n]^{2+}$ complexes with Am = en/2 or NH_3 the attenuation of the sideband intensities, expressed in terms of emreps, follows the pattern described by Eq. (31) [32,59]. There is appreciable scatter of the data for the complexes with L = $(Am)_4$ around the upper correlation line in Fig. 12 [32], and some significant deviations have been found upon a more extended, recent examination of the emission sidebands of $[Ru(Am)_4bpy]^{2+}$ complexes (Am = NH_3 or an aliphatic amine; lower set of complexes in Fig. 12) [79]. This work is discussed further below.

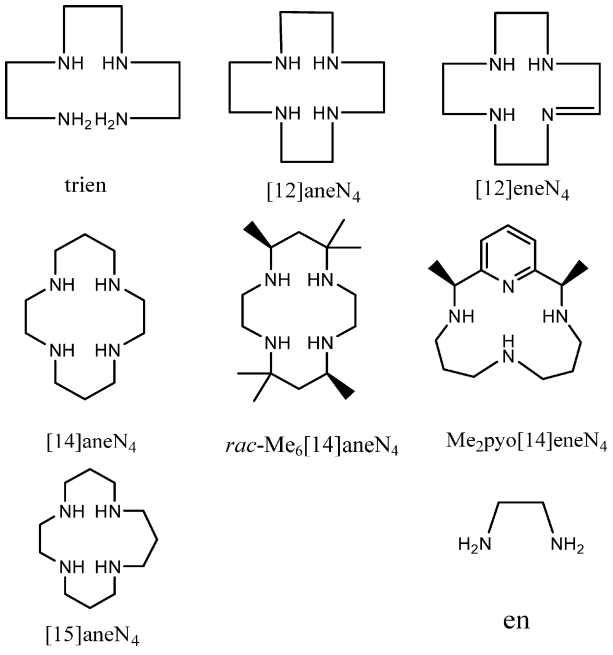

5.3. Evaluation of the contributions of the high frequency C–H and N–H stretching modes to MLCT excited state distortions

The highest frequency vibrational modes are expected, in principle, to provide very efficient excited state relaxation pathways [16,17,19]; however, this expectation, based on nuclear tunneling models, has not always been easy to reconcile with experimental observations on simple coordination complexes [20–26]. For example, our observation that $[Ru(NH_3)_4bpy]^{2+}$ does emit (in contrast to an earlier report [80]) at relatively long wavelength (12,500 cm^{-1}) and with a very short lifetime (25 ns) at 77 K might be considered an example of the effectiveness of the very high frequency N–H stretching modes in quenching a charge transfer excited state, but the observed isotope effect ($k_{NH}/k_{ND} \cong 3$ or an increase of lifetime of ∼0.17 per NH moiety) is smaller than expected for such a mechanism and in striking contrast to the 50-fold longer lifetime and larger isotope effect ($k_{NH}/k_{ND} \cong 14$ or ∼0.67 increase per NH moiety for a localized excited state) [39,49,81,82] for the metal-to-metal electron transfer emission of the trimetallic complex, *trans*-$[\{(NH_3)_5Ru^{II}(NC)\}_2Cr^{III}([14]aneN_4)]^{5+}$, which has a very similar emission energy. However, the tunneling probability is a function of the overlap of the vibrational wavefunctions of the two states, and thus of the displacement in the vibrational mode as well as its frequency [16,17]. It is therefore a concern that no contributions from such high frequency vibrational modes have been reported in rR studies [26,40,46]. The contributions of such vibrational modes are much easier to identify in emreps than in either the original emission [32,33,39,49] or the rR spectra; see Eqs. (18) and (19).

Careful comparisons emission spectra and emreps of the $[Ru(L)_4(d_8\text{-bpy})]^{2+}$ and $[Ru(L)_4(h_8\text{-bpy})]^{2+}$ isotopomers has permitted the detection of small in amplitude C–H vibronic components as the composite contributions of the correspond-

ing vibrational reorganizational energies [39,49]. The largest of these, $\Delta\Lambda_{x(\max)} = 25 \pm 10\,cm^{-1}$ at $h\nu_{x(\max)} \approx 2700\,cm^{-1}$, are found from the differences of isotopomer emreps for the complexes with $(L)_4 = (py)_4$ or $(bpy)_2$ and the C–H vibronic contributions are much smaller for $(L)_4 = (NH_3)_4$ [32,50]. However, the N–H vibronic contributions to the emission spectrum for these complexes are comparable to the noise level in the spectra and they are not unambiguously resolved ($\Delta\Lambda_{x(\max)} \leq 10 \pm 10\,cm^{-1}$, and λ_{NH} per NH may be less than $1\,cm^{-1}$ for the N–H stretching modes of the $[Ru(NH_3)_4bpy]^{2+}$ complex). Such small vibrational reorganizational energies lead to very small contributions of the highest frequency vibrational modes to the excited state relaxation rates in single mode/single relaxation channel models ($k_{nr}(calcd)/k_{nr}(obsd) \ll 10^{-4}$) [50].

In contrast, the spectral contributions of the N–H vibrational modes are well resolved in the differences between the emreps of the NH and ND isotopomers of the cyanide-bridged Cr^{III}–(CN^-)–Ru^{II} complexes with $\Delta\Lambda_{x(\max)} \approx 30\,cm^{-1}$ at $h\nu_{x(\max)} \approx 3200\,cm^{-1}$ [39,49]. Note that the value of $\Delta\Lambda_{x(\max)} \approx 30\,cm^{-1}$ is the composite contribution of all 19 N–H stretches since the values of ν_{NH} usually span a range of less than $400\,cm^{-1}$ [83] and this is smaller than $\Delta\nu_{1/2}$ (Table 2). Thus, for a localized, Cr^{II}–(CN^-)–Ru^{III} moiety in the excited state there are 19 N–H stretching vibrations, so the reorganizational energy per N–H stretching vibration is less than 30 but greater than $\sim 1.5\,cm^{-1}$. A value of λ_{NH} in the middle of this range could possibly account for the observed large isotope effect if all of the relaxation channels constructed from all possible combinations of the 19 N–H stretching modes contribute. The shorter lifetime and smaller isotope effect found for the $[Ru(NH_3)_4bpy]^{2+}$ complex, which has about the same excited state energy as the Cr–(CN)–Ru complex, apparently arise mostly from a combination of the smaller values of λ_{NH}, the smaller number of NH distortion modes and the intervention of some relaxation pathway that involves lower frequency vibrational modes such as the bpy skeletal modes [50].

5.4. Effects of the "spectator" ligands on the emission properties of the Ru–bpy chromophore

The emission band shapes of mono-bpy complexes are surprisingly varied. Thus, the $[Ru(NH_3)_4bpy]^{2+}$, $[Ru(en)_2bpy]^{2+}$, $[Ru(trien)bpy]^{2+}$ and $[Ru([12]aneN_4)bpy]^{2+}$ complexes have very similar values of $h\nu_{max(f)}$, but very different emission band shapes (Fig. 13) and excited state lifetimes [79]. This indicates that complexes with very similar ground state structures (Fig. 14), the same chromophore (Ru–bpy) and closely related ligands (tetraam(m)ines) can have very different MLCT excited state distortions. The simplest likely origin of this contrast in excited state structures is that the configurational mixing of the ^{3}MLCT excited state with a near in energy ^{3}LF excited state is smaller for the $[Ru([12]aneN_4)bpy]^{2+}$ complex than for the other $[Ru(Am)_4bpy]^{2+}$ complexes. Before that issue is considered further, it is important to consider how ground state perturbations of the bpy-ligand coordination affect the emission sideband intensity.

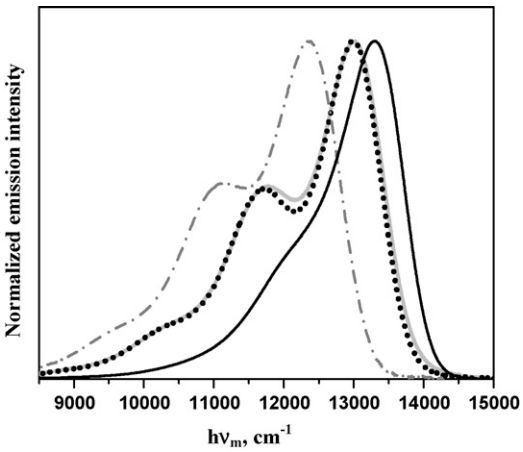

Fig. 13. Seventy-seven Kelvin emission spectra of the $[Ru(L)_4bpy]^{2+}$ complexes in butyronitrile with $(L)_4 = (NH_3)_4$ (gray dash-dot curve), trien (black dotted curve), $(en)_2$ (solid gray line) and $[12]aneN_4$ (solid curve), from [79].

In contrast to the nearly planar bpy ligands of the complexes compared in Fig. 14, the bpy ligand is appreciably twisted in the ground state of the $[Ru(Me_6[14]aneN_4)bpy]^{2+}$ complex; see Fig. 15. This is a result of the stereochemical repulsions with the methyl groups of the *rac*-$Me_6[14]aneN_4$ ligand. This complex has the largest emrep amplitude near $1500\,cm^{-1}$ of any of the complexes with similar absorption or emission maxima (compare especially $[Ru(Am)_4bpy]^{2+}$ complexes with $(Am)_4 = (en)_2$, trien, $[15]aneN_4$ and $[14]aneN_4$; Figs. 12 and 14). A larger reorganizational energy when the bpy ligand is twisted in the ground

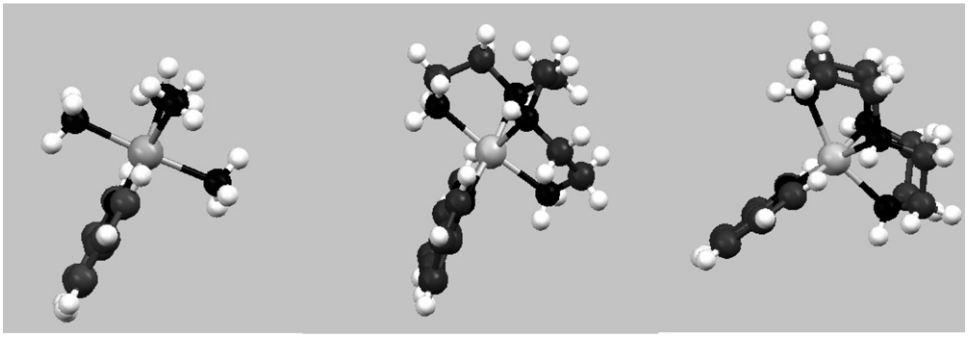

Fig. 14. X-ray structures (left to right) of $[Ru(NH_3)_4bpy]^{2+}$, $[Ru(trien)bpy]^{2+}$ and $[Ru([12]aneN_4)bpy]^{2+}$; [79].

Table 2
Electrochemical and emission spectral properties for simple transition metal complexes[a]

$[(L)_4Ru^{II}(PP)]^{2+}$, $[\{(L)_4Ru^{II}\}_2(PP)]^{4+}$	$E_{1/2}$ (V)[b]	$\Delta E_{1/2}$ (V)[c]	$h\nu_{max(abs)}$, $\langle\varepsilon/10^3\rangle$, $\{h\nu_{max(f)}, [\Delta\nu_{1/2}]\}$, 298 K[c]	$h\nu_{max(em)}$, 77 K	$h\nu_{max(f)}$, $[\Delta\nu_{1/2}]$, 77 K, $\{h\nu_{max(f)}, [\Delta\nu_{1/2}]\}$, 298 K	Λ_x (ν_x), 77 K
$[(bpy)_2Ru(bpy)]^{2+}$	1.27–1.34	2.61	21.9 (d/w) 22.1, ⟨12.4⟩, {22.1, [2.2]}[c]	17.12 (d/w) 17.25	17.22 [0.68] (d/w), 17.31 [0.64]	1.16 (1.49) (d/w), 1.05 (1.50)
$[(bpy)_2Ru(phen)]^{2+}$	1.32–1.29	2.61	22.2, ⟨14.5⟩, {22.1 [2.3]}	17.25	17.33 [0.68]	1.09 (1.51)
$[(bpy)(en)Ru(bpy)]^{2+}$	1.00–1.42	2.42	20.2 (d/w) 20.4	15.00 (d/w) 15.11	15.06 [0.78] (d/w), 15.16 [0.72]	1.00 (1.50) (d/w), 0.88 (1.49)
$[(bpy)(NH_3)_2Ru(bpy)]^{2+}$	0.95–1.44	2.39	20.4 (d/w) 20.2	14.56 (d/w) 14.67	14.64 [0.91] (d/w), 14.70 [0.78]	0.99 (1.53) (d/w), 0.86 (1.49)
$[(py)_4Ru(bpy)]^{2+}$	1.38–1.32	2.70	22.6, ⟨5.9⟩, {22.5 [2.4]}	16.87	16.91 [0.89]	0.90 (1.40)
$[([12]eneN_4)Ru(bpy)]^{2+}$	0.84–1.58	2.42	20.1, ⟨5.3⟩, {20.1 [3.1]}	14.49	14.56 [0.91]	0.57 (1.34)
$[(Me_2pyo[14]eneN_4)Ru(bpy)]^{2+}$	0.88–1.52	2.40	20.1, ⟨5.3⟩, {20.1 [3.1]}	14.49	14.56 [0.91]	0.57 (1.34)
$[(rac\text{-}Me_6[14]aneN_4)Ru(bpy)]^{2+}$	0.87–1.54	2.41	19.3, ⟨4.5⟩, {19.4 [2.6]}	13.97	14.04 [0.89]	0.86 (1.47)
$[([14]aneN_4)Ru(bpy)]^{2+}$	0.85–1.55	2.40	19.0 (d/w) 19.5, ⟨5.0⟩, {19.5 [2.3]}	13.96 (d/w) 13.99	14.01 [0.95] (d/w), 14.03 [0.89]	0.85 (1.44) (d/w), 0.81 (1.45)
$[([15]aneN_4)Ru(bpy)]^{2+}$	0.84–1.51	2.35	19.3, ⟨4.5⟩, {19.3 [2.0]}	13.60	13.63 [0.89]	0.78 (1.45)
$[([12]aneN_4)Ru(bpy)]^{2+}$	0.70–1.58	2.28	19.1, ⟨4.5⟩, {19.5 [2.6]}	13.31	13.37 [0.83]	0.48 (1.31)
$[(trien)Ru(bpy)]^{2+}$	0.68–1.59	2.27	19.5, ⟨4.6⟩, {19.5 [2.1]}	13.00	13.02 [0.87]	0.76 (1.43)
$[(en)_2Ru(bpy)]^{2+}$	0.68–1.62	2.30	19.1 (d/w) 19.2, ⟨4.7⟩, {19.2 [2.1]}	12.82 (d/w) 13.01	12.88 [1.03] (d/w), 13.05 [0.89]	0.85 (1.45) (d/w), 0.78 (1.45)
$[(NH_3)_4Ru(bpy)]^{2+}$	0.61–1.64	2.25	18.9 (d/w) 19.0, ⟨4.0⟩, {19.0 [2.1]}	12.02 (d/w) 12.37	12.09 [1.11] (d/w), 12.42 [0.92]	0.81 (1.45) (d/w), 0.80 (1.48)
$[(bpy)_2Ru(dpp)]^{2+}$	1.415–1.029	2.45	21.2, ⟨10.9⟩ (d/w) 21.5, ⟨11.8⟩	16.20	16.30 [0.87]	0.84 (1.50)

[a] All energies in units of $cm^{-1}/10^3$. In butyronitrile glass except as indicated; d/w = DMSO/water. Data from [32,49,50,59,70,79].
[b] In acetonitrile, scan rate = 100 mV/s, ref. = Ag/AgCl, $E_{1/2}(ferrocene^{+1/0}) = 0.437$ V.
[c] $\Delta E_{1/2} = E_{1/2}\ (Ru^{3+/2+}) - E_{1/2}\ (PP^{0/-1})$.

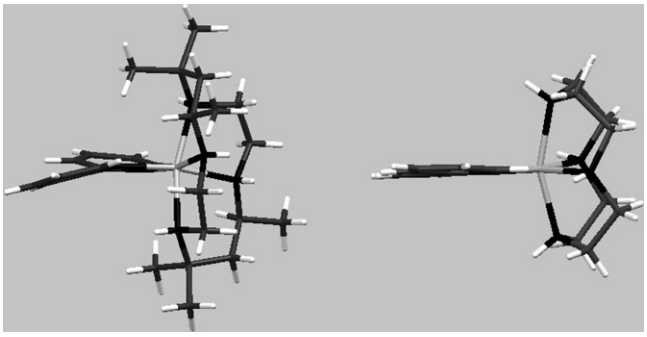

Fig. 15. Comparison of the twist of the bpy ligands in the X-ray structures of $[Ru(rac\text{-}Me_6[14]aneN_4)bpy]^{2+}$ (left) and $[Ru([12]aneN_4)bpy]^{2+}$ (right) [79].

state suggests that this ligand tends to be planar in the MLCT excited state, at least around the 2,2′-linkage of the pyridyl moieties, and this is consistent with a model in which for the electron equally distributed over the pyridyls in the bpy-LUMO of the MLCT excited state.

A systematic comparison of emreps (Fig. 12) indicates that most exhibit the systematic decrease in excited state distortion with decreasing excited state energy that is expected for ground state–excited state configurational mixing in a simple two state model, but the complexes with $(L)_4$ = [12]aneN$_4$, [12]eneN$_4$ and $(py)_4$ all have less distorted excited states than related complexes with the same emission energy. The observations are not consistent with simple two state models and seem to require an additional distortion induced by excited state–excited state configurational mixing in most of the complexes. When configurational mixing between two excited states (e and e′) is important, the distortions of the highest energy excited state will be mixed with those of the lowest energy excited state. Therefore, Eqs. (27) and (28) must be modified when configurational mixing among excited states is important, and the effect on the observed vibronic contributions to sideband intensities for the $\{e, 0\} \rightarrow \{g, k\}$ transition can be expressed as [79]:

$$\lambda_k \approx \lambda_{k(0)} \left(1 - 2\alpha_{ge}^2 - 2\alpha_{eg}^2 + 2\alpha_{ee'}^2 \sqrt{\frac{\lambda_{k(e')}}{\lambda_{k(e)}}} \right)_k \quad (34)$$

Since the stereochemical constraints of the coordinated [12]aneN$_4$ ligand tend to restrict the amplitudes of tetragonal distortions around the metal, one expects a relatively high energy and less shifted PE minimum for this ^{3}LF excited state than for those with less constrained ligands. A smaller displacement of PE minima results in a smaller value of $\lambda_{k(e')}$ for the more constrained ligands, and therefore smaller amplitudes for the first and second order contributions to the correlated vibronic sidebands. While this model of ^{3}LF/^{3}MLCT configurational mixing provides a plausible account for the relatively small values of $\Lambda_{x(max)}$ at about 1500 cm^{-1} for the $[Ru([12]aneN_4)bpy]^{2+}$ and $[Ru([12]eneN_4)bpy]^{2+}$ complexes, it can account for the observations on $[Ru(py)_4bpy]^{2+}$ only if the PE minimum for the ^{3}LF excited state has approximately the same nuclear coordinates but a significantly higher energy (compared to $H_{CT,LF}$ and resulting in a smaller value for $\alpha_{ee'}$) than that for $[Ru(bpy)_3]^{2+}$. This may be the case, but there other origins of the relatively weak vibronic sidebands found for this complex may be possible (e.g., configurational mixing with a low energy Ru/py MLCT excited state), and this is being further investigated.

5.5. Summary and overview of observations on monometallic complexes

The band shapes of the $[Ru(NH_3)_4bpy]^{2+}$ and $[Ru(bpy)_3]^{2+}$ emission spectra at 77 K in frozen solutions are well accounted for by a Gaussian model for vibronic progressions in the distortion modes identified in the rR studies of these complexes [32]. Furthermore, the rR data on these complexes provide a basis for modeling the vibronic contributions to emission band shapes, uncertainties in all aspects of the emission sideband analysis described here, and approximate corrections as functions of bandwidth have been obtained [32]. Since the errors are systematic in $\Delta\nu_{1/2}$, it is often necessary to correct for intrinsic bandwidth differences in the direct comparison of observed parameters in a series of related complexes.

The systematic comparison of the emission band shapes of a series of complexes is facilitated by constructing reorganizational energy profiles (emreps) from the resulting difference emission spectra since these profiles make more evident the variations in excited state displacements (more correctly, the amplitudes of the emreps are functions of the squared displacements). The modeling based on rR parameters has also been used to validate this procedure and explore its implications [32], and the approaches described here are most useful when the fundamental component is the most intense spectral component and when the component bandwidths are less than about 1500 cm^{-1}. Since the fundamental component of the Ru–bpy complexes comprises most of the intensity of their emission spectra near to the emission maxima, the uncertainties for the difference emission spectra and the emreps are very large for vibronic contributions which have small vibrational frequencies; therefore, spectral variations in the region $h\nu_d = (h\nu_{max(f)} - h\nu_m) < 500\,cm^{-1}$ have not been considered in this discussion.

The examination of band shapes in an extended collection of $[Ru(L)_4bpy]^{2+}$ complexes has provided new insights into the properties of their lowest energy electronic excited states: (a) the vibronic components in the $[Ru(L)_4bpy]^{2+}$ complexes are increasingly attenuated as the excited state energy decreases, in a manner that is consistent with appreciable excited state–ground state configurational mixing; (b) ground state distortions of the bpy ligand result in increased intensity of the vibronic contributions to the emission band shape, consistent with expectation based on the bpy LUMO as the acceptor; (c) manipulation of the "spectator" $(L)_4$ ligands can result in large alterations of the emission band shape that are not readily attributable to stereochemical constraints on the ground state, but are consistent with alterations of LF excited state distortions and energies and, consequently, these effects appear to implicate configurational mixing between the ^{3}MLCT and ^{3}LF excited states as an important contribution to the ^{3}MLCT excited state distortion of most $[Ru(L)_4bpy]^{2+}$ complexes.

6. The use of emreps to explore CT excited state properties in bi- and tri-metallic complexes

6.1. General considerations

The analysis of emission band shapes as described in Section 3 above should be very general if a good estimate of the fundamental component can be made. In particular and the attenuation of vibronic sideband intensity implied by Eqs. (30) and (31) and demonstrated for $[Ru(L)_4bpy]^{2+}$ complexes suggests that these approaches might be useful in the experimental examination of issues such as the distortions in high frequency vibrational modes, the excited state distribution of electron density, etc., in multi-metallic complexes. Some recent studies of the emission band shapes of bi- and tri-metallic complexes [39,49,70] are summarized here.

6.2. Excited state–excited state electronic coupling in bis-Ru(II) complexes with mixed valence excited states

The MLCT excited states of bimetallic, bis-ruthenium(II) complexes with PP bridging ligands (B) are formally mixed valence excited states, with each of the degenerate diabatic MLCT excited states containing one Ru(II) and one Ru(III) center. If the electronic coupling between the Ru(II) and Ru(III) centers is very strong, then the vibronic contributions to the emission sideband intensity should be much smaller than in the limit in which the there is no Ru(II)/Ru(III) electronic coupling (U); this is qualitatively illustrated in Fig. 16 and it may be expressed in terms of different contributions to the respective emreps (note that excited state–ground state configurational mixing will not shift the ground state PE minimum of the symmetrical bimetallic complexes in the limit of a single distortion mode) [70]:

$$\Lambda_{x(\max;U)} \cong \Lambda^{\circ}_{x(\max;U)}(1 - 2\alpha^2_{ge} - 2\alpha^2_{eg}) \cong \Lambda^{\circ}_{x(\max;U)}(1 - n_{e(U)}\alpha^2_{eff(U)}) \quad (35)$$

$$\Lambda_{x(\max;B)} \cong \Lambda^{\circ}_{x(\max;B)}(1 - 2\alpha^2_{eg} - 4\alpha^2_{ee'}) \cong \Lambda^{\circ}_{x(\max;B)}(1 - n_{e(B)}\alpha^2_{eff(B)}) \quad (36)$$

The limit of no Ru(II)/Ru(III) electronic coupling is better formulated as the limit in which there is no configurational mixing between the degenerate $\{Ru^{II}, Ru^{III}\}$ and $\{Ru^{III}, Ru^{II}\}$ excited states. This limit may be approximated by the monometallic $[Ru(L)_4PP]^{2+}$ complexes, and their spectra may be considered as the reference for the evaluation of the spectral effects of configurational mixing between the degenerate $\{Ru^{II}(PP^{-})Ru^{III}\}$ and $\{Ru^{III}(PP^{-})Ru^{II}\}$ MLCT excited states.

The emreps obtained from the emission spectra of several $[Ru(L)_4PP]^{2+}$ and $[\{(L)_4Ru\}_2PP]^{4+}$ complexes are compared in Fig. 17. The vibronic intensities of the $[Ru(bpy)_2PP]^{2+}$ complexes with PP = bpm, dpq and dpb (see Glossary) are attenuated with decreasing excited state–ground state energy differences in the same manner as the $[Ru(L)_4bpy]^{2+}$ complexes. This indicates that the effective or averaged vibrational reorganizational energy contributions of the PP and bpy ligand distortions are similar and

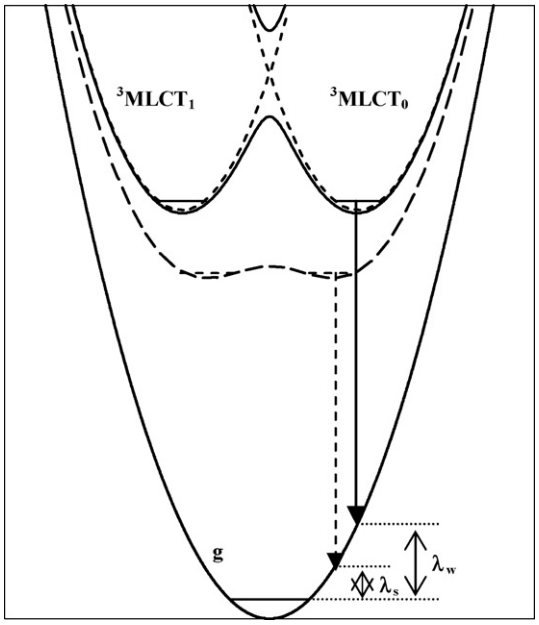

Fig. 16. Qualitative illustration of the attenuation of reorganizational energy that is expected to result from the configurational mixing between excited states. The diabatic (unmixed) excited states are indicated the short dashed curves, the lowest energy PE surface generated by weak configurational mixing of the excited states by the solid line and strong configurational mixing is designated by the curve with long dashes. The reorganizational energies are λ_w for weak configurational mixing and λ_s for strong configurational mixing of excited states. The excited state PE curves do not take into account the effects of configurational mixing with the ground state.

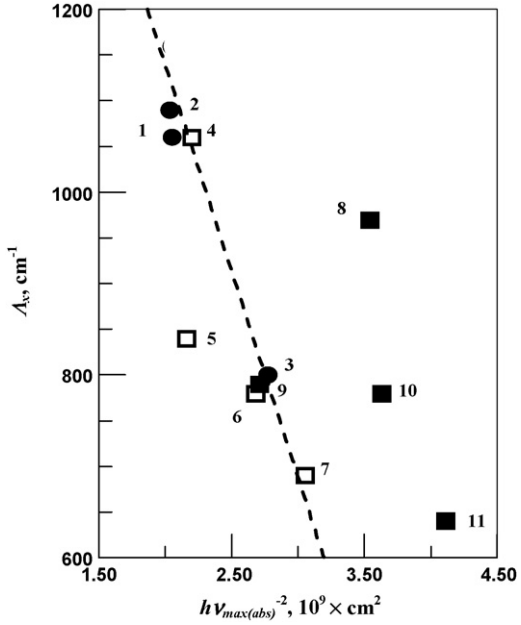

Fig. 17. Reorganizational energy attenuation of $[Ru(bpy)_2PP]^{2+}$, $[\{Ru(bpy)_2\}_2PP]^{2+}$ and $[Ru(NH_3)_4bpy]^{2+}$ complexes based on Eq. (31). Reference complexes: PP = bpy, 1; PP = phen, 2; $[Ru(NH_3)_4bpy]^{2+}$, 3. Monomers with PP = bpm, 4; dpp, 5; dpq, 6; dpb, 7. Dimers with PP = bpm, 8; dpp, 9; dpq, 10; dpb, 11. Data for $[Ru(NH_3)_4bpy]^{2+}$ are from [79], for $[Ru(bpy)_2PP]^{2+}$ and $[\{Ru(bpy)_2\}_2PP]^{2+}$ are from [70] and the line is drawn consistent with the reorganizational energy attenuation of the $[Ru(Am)_{6-2n}(bpy)_n]^{2+}$ complexes as reported in [40]. The data are not corrected for differences in bandwidth, Fig. 8 in [70].

that the electronic matrix elements for ground state–excited state configurational mixing are also very similar. The complex with PP = dpp deviates from this pattern most likely because the dpp LUMO correlates with LUMO + 1 of dpq, dpb and pyrazine [44], and the differences in orbital coefficients imply different electronic distributions and distortions for these different π^* orbitals.

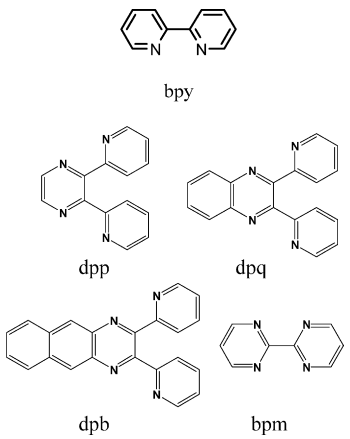

Based on Fig. 16 and Eq. (36), very strong configurational mixing between the degenerate MLCT excited states of the PP-bridged bimetallic complexes should result in $\Lambda_{x(\max;B)} < \Lambda_{x(\max;U)}$; thus, if the electronic coupling were the same in the ground and excited states, then the observation that $F\Delta E_{1/2} \approx 0.18$ eV (1500 cm^{-1}) in the ground state, together with estimates of a 0.03 eV electrostatic contribution and reorganizational energy of ~6000 cm^{-1} for mixed valence electron transfer in these complexes [70], implies $H_{ee'} \sim 1400\,\mathrm{cm}^{-1}$; this corresponds to $4\alpha^2_{ee'} \sim 0.2$, or 20% attenuation from this effect in addition to the very large attenuation expected to result from configurational mixing with the ground state due to the small excited state–ground state energy difference. This attenuation is not observed for either $(L)_4 = (bpy)_2$ [70] or $(NH_3)_4$ [84]. Rather, we find that $\Lambda_{x(\max;B)} \sim \Lambda_{x(\max;U)}$ for all these mono- and bi-metallic complexes, and since $h\nu_{\max(f;B)} \ll h\nu_{\max(f;U)}$ the resulting differences in vibronic attenuation, Eqs. (35) and (36), imply that $\Lambda_{x(\max;B)} > \Lambda_{x(\max;U)}$ when corrected to the same value of $h\nu_{\max(f)}$. These considerations imply that the $Ru^{II}(PP)Ru^{III}$ ground states of these complexes are more delocalized than their $Ru^{II}(PP^-)Ru^{III}$ excited states. This inference is consistent with observations on the ground state absorption spectra of the complexes with $(L)_4 = (bpy)_2$ [70]: (a) the comparable splitting between the two Ru^{II}/Ru^{III} oxidation peaks found in the electrochemistry of all of the bimetallic complexes implies that there should be two Ru/PP MLCT transitions (i.e., a Jahn–Teller like splitting of the MLCT transition) separated by $\sim 2H_{ee'} \sim 3000\,\mathrm{cm}^{-1}$; (b) the single MLCT peak observed in the bimetallic complexes has twice the absorptivity of the MLCT transition in the corresponding $[Ru(L)_4PP]^{2+}$ complexes. The ground state coupling is consistent with a PP–ligand mediated electron transfer super-exchange mechanism [70], but two super-exchange mechanisms should be considered for the excited state coupling: (a) (PP^-)-mediated electron transfer mechanism; (b) a $^3LF(Ru^{II})$ excited state mediated hole transfer mechanism. If the MM′ coupling is by means of the partly occupied PP-LUMO, then the mediating excited state (formally, a $Ru^{III}(PP^{2-})Ru^{III}$ MLCT state), whether the mediating PP-orbital is the singly occupied-LUMO or the LUMO + 1 of the ground state, is higher energy in the excited state than is the mediating LUMO of the ground state and there is correspondingly less configurational mixing of the degenerate electronic configurations. For a hole transfer mechanism, $E^{0'0''}_{CT,LG}$ may be relatively large and poor π/σ orbital overlap may lead to small values of $H_{CT,LF}$ so that H^{spx}_{01} is very small (see discussion in Section 4.3.2). Thus, the surprisingly large emrep amplitudes for the PP-bridged bimetallic complexes are readily interpreted in terms of: (a) relatively localized MLCT excited states, with very small values of $\alpha^2_{ee'}$; (b) the absence of any significant shift of the ground state PE minima for the bimetallic complexes (i.e., relatively small contribution of a α^2_{ge} term to the attenuation in Eq. (33)). The amplitudes of the relatively intense vibronic sidebands observed for the $[\{(L)_4Ru\}_2PP]^{4+}$ complexes do decrease in amplitude as the excited state energy decreases even though excited state/ground state configurational mixing should not alter the nuclear coordinates of the ground state PE minimum ($\alpha^2_{ge} \approx 0$). This indicates that there is significant ^{3}MLCT/ground state configurational mixing in these complexes ($\alpha^2_{eg} > 0$) [84].

6.3. Studies of transition metal–transition metal electron transfer excited states: cyanide-bridged Cr(III)–Ru(II) complexes

Several bimetallic and trimetallic complexes in which cyanide bridges chromium(III) and ruthenium(II) have been found to emit in the near infrared [39,49,82]. These emissions have been identified as $\{Ru^{III}Cr^{II}\} \rightarrow \{Ru^{II}Cr^{III}\}$ electron transfer or MMCT emissions, and these are the first such emissions reported. Thus, the complexes for which the donor is a ruthenium(II)am(m)ine have an intense $\{Ru^{II}Cr^{III}\} \rightarrow \{Ru^{III}Cr^{II}\}$ absorption band ($\varepsilon_{max} \cong 4000\,M^{-1}\,cm^{-1}$ per Ru(II)) between 15,000 and 22,000 cm^{-1} [85–89] and a weak emission between 10,000 and 13,000 cm^{-1} [39,49,82]. All of the parent mono-chromium complexes exhibit a Cr^{III}-centered ligand field excited state emission, ^{2}E (or ^{2}LF), the range of 12,500–14,700 cm^{-1} [53,90–93]; e.g., see Fig. 2. Similar ^{2}LF excited states are expected in the $\{Ru^{II}Cr^{III}\}$ complexes, and the ^{2}LF energies are very close to those assigned as MMCT emissions. A substantial number of $\{Ru^{II}Cr^{III}\}$ complexes have been examined [49,70,82,94,95] and the MMCT-type of emission is only observed in complexes in which Ru^{II} is a good electron transfer donor (i.e., a reasonably good reducing agent). For weak electron donors (as in a Ru^{II}–PP complex) only the ^{2}E emission is observed [94,95]. Even in those complexes that exhibit the MMCT emission, its spectroscopic characterization is often complicated by the ^{2}LF emission. Thus, the observed emission is dependent on the excitation wavelength; in general, excitation on the low energy side of the MMCT absorption produces clean MMCT emissions and excitation at energies higher than the MMCT maximum produce spectra broadened at high energies, or sometimes new emission bands, and the excited state decays are at least bi-exponential with the higher energy component being somewhat longer lived [39,49,82]. These properties are

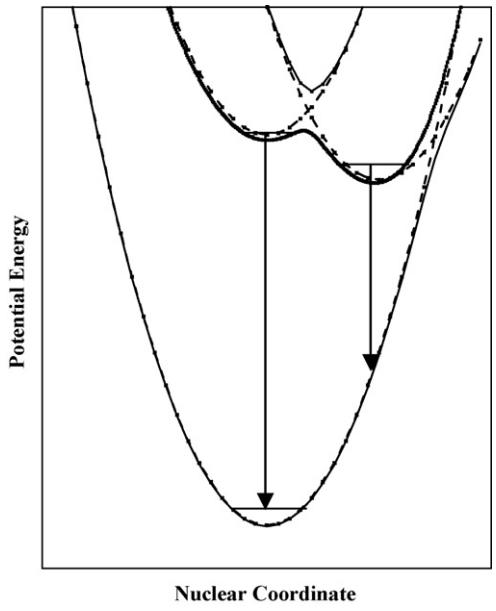

Fig. 18. Qualitative PE curves illustrating a system with two configurationally mixed electronic excited states, such as found in Cr(CN)Ru complexes.

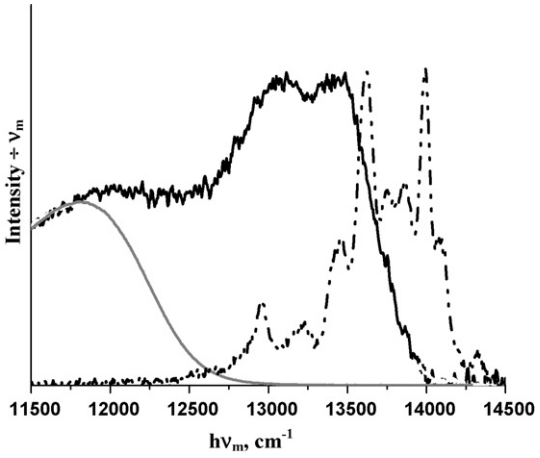

Fig. 19. Emission spectra of *trans*-[{$(NH_3)_5RuNC$}$_2$Cr(*m*-Me_6[14]aneN_4)]$^{5+}$ isotopomers at 77 K in DMSO–water glasses: proteo (NH) complex, black line, irradiated at 395 nm; deutereo (ND) complex, grey line, irradiated at 532 nm. The emission sectrum that results from the 420 nm irradiation of *trans*-[Cr(*m*-Me_6[14]aneN_4)$(CN)_2$]$^{2+}$ under the same conditions is shown by the dash-dot-dot curve. The emission maxima of the different spectra have been adjusted to facilitate comparison. Spectra from [39].

reasonably consistent with ^{2}LF and MMCT excited states that are very close in energy (the PE minima probably differ in energy by less than about 3000 cm^{-1}) as illustrated in Fig. 18, and with the probability for populating each state depending on the excitation energy. The emission of the [{$(NH_3)_5RuNC$}$_2$Cr(*m*-Me_6[14]aneN_4)]$^{5+}$ complex is instructive in this regard as we have been able to approximately resolve the two emission components and the higher energy component is similar to, but red-shifted by about 570 cm^{-1} and broader than the emission of the [Cr(*m*-Me[14]andN_4)$(CN)_2$]$^+$ parent; see Fig. 18. These two electronic states are analogous to the mixed valence excited states discussed in the previous section, for example:

$$^2\{^2Cr^{III}, {}^1Ru^{II}\} \leftrightharpoons {}^2\{^3Cr^{II}, {}^2Ru^{III}\} \quad (37)$$

and the shift to lower energy and the broadening of the ^{2}E component are expected consequences of configurational mixing between $^2\{^2Cr^{III}, {}^1Ru^{II}\}$ and $^2\{^3Cr^{II}, {}^2Ru^{III}\}$.

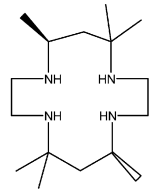

ms-Me_6[14]aneN_4

The reorganizational energy profiles derived from the MMCT emission spectra of the Cr^{III}–(CN)–Ru^{II} complexes have maximum amplitudes, $\Lambda_{x(max)}$, of 350–500 cm^{-1} for vibrational frequencies of $\nu_{x(max)}$ = 800–1000 cm^{-1} [39,49,82]; these frequencies are consistent with coordination sphere distortions dominating the Ru/Cr electron transfer process. A shoulder is also resolved in the emreps at $h\nu_x \cong 2000$ cm^{-1}, implicating the C–N stretching vibration, and the weak contributions of NH vibronic sidebands have been resolved by comparing the reorganizational energy profiles of the proteo (NH) and deutereo (ND) am(m)ine isotopomers [39,49,82] (Fig. 19).

The relatively small amplitude of $\Lambda_{x(max)}$, smaller than observed for most [Ru(L)$_4$bpy]$^{2+}$ complexes, suggests relatively little excited state distortion and this is more consistent with a Cr(dπ) → Ru(dπ) transition than with a Cr(dσ) → Ru(dπ) transition; thus, in these complexes the Huang–Rhys factors are necessarily very small, $S_k \ll 1$, while the distortions that accompany changes in the population of dσ-orbitals in monometallic complexes typically have $S_k \gg 1$ [66,96,97]. Although the emreps do not permit identification of the specific distortion modes, comparison of emreps of the NH/ND isotopomers suggests that M–N–H rocking modes and H–N–H bending modes make small contributions to the emission band shape [49]. The reorganizational energies attributable to the NH-stretching modes, $\Lambda_{NH} \cong 30$ cm^{-1}, is much smaller than the values observed for $\Lambda_{x(max)}$ which is attributable to the lower frequency vibrations. However, the value of Λ_{NH} found may be consistent with a tunneling pathway for the back electron-transfer and the large observed NH/ND isotope effects if all of the N–H stretching modes contribute and their combinations result in a very large number of relaxation channels (>10^4), each of which contributes a small amount to the overall non-radiative relaxation rate.

7. Some implications for inverted region electron transfer rate constants

The non-radiative relaxation of the CT excited state in these systems is an electron transfer process in the Marcus inverted region [3] and the molecular parameters that govern the non-radiative electron transfer relaxation are the same parameters that contribute to the emission spectrum [9,14,33], the inferences summarized here have implications for the Marcus inverted region electron transfer processes. Furthermore, most of the solvent vibrational modes are frozen in 77 K solutions [8] so that

$\lambda_{solv} \ll 1000\,cm^{-1}$ and $RT = 53\,cm^{-1}$ for the systems described. As a consequence, thermally activated processes are relatively unimportant and the rate constant for inverted region electron transfer depends on the isoenergetic nuclear tunneling from {e, 0′} to populate relaxation channels that are comprised of higher order harmonics or combinations of ground state distortion modes. The relaxation rate constant for any one channel (c) may be formulated in a manner analogous to that used for a single distortion mode [9,16–18,98,99]:

$$\frac{(k_{et})_c}{A} \approx \left[\frac{1}{N_c!}\prod_k \left(\frac{\lambda_k}{h\nu_k}\right)^{n_k}\right][e^{-\{G_c^2/4RT\lambda_s\}}] \quad (38)$$

with $G_c = [|\Delta G_{eg}| - \lambda_s - \sum_k n_k h\nu_k]$, $(n_1 + n_2 + n_3 + n_4 + \cdots) = N_c$, and

$$A \approx \frac{2\pi^2}{h}\frac{H_{eg}^2}{(\pi\lambda_s k_B T)^{1/2}} \quad (39)$$

The equivalent to Eq. (38) in the single distortion mode limit is simply [9,16–18,98,99]:

$$\frac{(k_{et})_j}{A} \approx \left[\frac{1}{j!}\left(\frac{\lambda}{h\nu}\right)^j e^{-\{G_c^2/4RT\lambda_s\}}\right] \quad (40)$$

The net relaxation rate constant is obtained by summing over all channels: c in Eq. (38) and j in Eq. (40). In the limit of low temperatures, Eq. (38) can be simplified since most solvent modes are frozen ($\lambda_s \to 0$), $k_B T$ is very small ($53\,cm^{-1}$ at 77 K) and $|\Delta G_{eg}| \cong h\nu_{max(f)} \geq 12{,}000\,cm^{-1}$, so the exponential factors act like delta functions centered around possible relaxation channels; in this limit, each channel corresponds to frequencies such that $\sum_k n_k\nu_k \approx (E^{0'0} \pm k_B T)$. Under these circumstances, harmonics of the highest frequency vibrational modes are strongly favored as relaxation channels when there are significant displacements in these modes [16,17]. However, the displacements in the highest frequency vibrational modes (the C–H and N–H stretching frequencies) of the $[Ru(L)_4bpy]^{2+}$ complexes are too small for their harmonics to be the dominant relaxation channels, and $h\nu_k$ and λ_k for the mid-range distortion modes of the bpy ligand (C–C and C–N stretches) are sufficiently small that the harmonics of any such mode cannot account for 0.1% of the observed relaxation rate constant [32,33,50,79]. However, there are more than 11 distortion modes identified in the rR spectra of these complexes, and a very large number ($\gg 10^6$) of relaxation channels are possible even in the low temperature limit.

There has, of course, been considerable discussion of many of the issues related to excited state relaxation and inverted region electron transfer, and some comparison of the implications of our observations with some of the previous studies is appropriate. Probably the most relevant of these earlier studies is the work of the Meyer group [12,20,23–26,100–106]. This work has focused mostly on ambient spectra and lifetimes which are evaluated in terms of a master equation representing the vibronic contributions. These authors represent the actual spectra and lifetime data by a single "equivalent" distortion mode in the frequency range characteristic of the bpy skeletal modes. This model contrasts to a multi-mode model implied by the small amplitude distortions in many modes found in the rR studies [26,40,46]. Although, we have been unable to find any single mode model that properly represents the observed 77 K band shapes [33] because of the significant contributions of low frequency vibrational modes combined with the significant contributions of their second order vibronic components to the spectra in the region of greatest sideband intensity, the discrepancies between the observed spectra and single mode models seem to decrease as the spectral bandwidth increases. Furthermore, the values of $\Lambda_{x(max)}$ and ν_x found in our studies do give a reasonable representation of the variations in excited state lifetimes at a single temperature when substituted for the reorganizational energy and frequency of a presumed single distortion mode [32,33,50], and this is consistent the previous observations on the use of single mode models [12,20,23–26,100–106]. Since $\Lambda_{x(max)}$ has been clearly clearly shown to be a composite quantity, the equivalent parameters used in single mode fittings must also be some composite of the contributions of many overlapping first, second and possibly higher order vibrational modes and the physical significance of such single mode fitting parameters is not clear. On the other hand, our observations that the vibrational reorganizational energies are very small for the high frequency C–H and N–H stretching modes of the Ru–bpy complexes do support the previous arguments that "medium" frequency vibrational modes, in the 1200–1650 cm^{-1} range, are more important than the high frequency vibrational modes in determining the MLCT excited state lifetimes of the Ru-bpy complexes.

8. Conclusions

8.1. General

This article has emphasized a systematic approach to the interpretation of variations in CT emission band shapes for complexes in which the ground state and the excited state do not differ greatly in their molecular structures, and the applications of this approach to some series of related complexes. The basic premise of our approach is that the emission envelope can be represented as the sum over a fundamental component and vibronic components corresponding to vibrational progressions in all of the displacement modes. Reorganizational energy profiles are proving to be convenient and useful tools for systematically comparing variations in the excited state structures of a series of related complexes. Their usefulness derives from the fact that their amplitudes are functions of the vibrational reorganizational energies, λ_k (or squared displacements) of the vibrational displacement modes and changes in emrep amplitudes in related complexes follow closely the correlated changes in vibrational reorganizational energies; in contrast, the amplitudes of spectroscopic sidebands are functions of (λ_k/ν_k).

8.2. MLCT excited state properties for some mono- and multi-metallic complexes inferred from emissionband shape variations

8.2.1. $[Ru(L)_4bpy]^{2+}$ complexes

The emreps have demonstrated a marked attenuation of vibronic sideband intensity in a related series of $[Ru(L)_4bpy]^{2+}$

complexes due to changes in ground state–excited state configurational mixing as the excited state energy becomes smaller; thus, the maximum emrep amplitude of $[Ru(bpy)_3]^{2+}$ is about twice that of $[Ru(NH_3)_4bpy]^{2+}$ and in reasonably good agreement with expectations based on simple perturbation theory arguments. Similar attenuation effects have been found for other $[Ru(L)_4PP]^{2+}$ complexes. This attenuation arises mostly from shifts of the PE minima closer to one another as a consequence of configurational mixing, it is heavily weighted in the squared mixing coefficient and such attenuation is expected when the corresponding electronic matrix elements are large (e.g., as manifested in very intense MLCT absorption bands). Furthermore, it seems likely that such vibronic sideband attenuation might eventually become useful as an experimental measure of the extent of configurational mixing.

By using emreps in combination with the emission spectra of CH/CD isotopomers it has been possible to identify the very weak vibronic contributions of the C–H stretching modes in several of the $[Ru(L)_4bpy]^{2+}$ complexes. The vibrational reorganizational energies of these distortion modes are probably too small to be detected by most other techniques or to be the only contributions to channels for MLCT excited state relaxation.

The stereochemical restrictions on coordination sphere distortions imposed by the [12]aneN$_4$ and [12]eneN$_4$ ligands result in unusually large attenuation of emission sideband intensities, and this may correspond to smaller vibronic contributions arising from the configurational mixing of a ligand field excited state with the emitting ^{3}MLCT excited state in these than in most Ru–bpy complexes.

8.3. Variations in vibronic sideband intensities of the CT emission spectra of bimetallic and trimetallic transition metal complexes

The $[\{Ru(L)_4\}_2PP]^{4+}$ complexes (L = $(bpy)_2$ or $(NH_3)_4$) all emit at lower energies than their mono-metallic parents and allowing for the differences in attenuation expected for these energy differences, the bimetallic complexes all have much more vibronic sideband intensity than expected. This implies that the electron density in the Ru^{II} and Ru^{III} centers of the mixed valence excited states in these complexes is more localized than in the related mixed valence ground states.

The vibronic sidebands of the MMCT emission spectra of $Cr^{III}(CN)$–Ru^{II} complexes are relatively weak and the most intense contributions are less than 1000 cm^{-1} lower in energy than the maximum of the fundamental component. Thus, the emrep amplitudes found for $[\{Ru(NH_3)_5\}_2Cr([14]aneN_4)]^{5+}$ are consistent with very small differences in coordination sphere bond lengths and angles accompanying the electron transfer process, and this suggests that the Cr(II) center in the excited state has a $d\pi^3$ electronic configuration.

Acknowledgement

The authors thank the Office of Basic Energy Sciences of the Department of Energy for partial support of this research.

References

[1] N.S. Hush, Electrochim. Acta 13 (1968) 1005.
[2] N.S. Hush, Prog. Inorg. Chem. 8 (1968) 391.
[3] R.A. Marcus, Annu. Rev. Phys. Chem. 15 (1964) 155.
[4] R.S. Mulliken, W.B. Person, Molecular Complexes, Wiley-Interscience, New York, 1967.
[5] N.S. Hush, in: D.B. Rorabacher, J.F. Endicott (Eds.), Mechanistic Aspects of Inorganic Reactions, ACS Symposium Series 198, American Chemical Society, Washington, 1982.
[6] N. Sutin, Acc. Chem. Res. 15 (1982) 275.
[7] C. Creutz, Prog. Inorg. Chem. 30 (1983) 1.
[8] R.A. Marcus, J. Phys. Chem. 94 (1990) 4963.
[9] I.R. Gould, D. Noukakis, L. Gomez-Jahn, R.H. Young, J.L. Goodman, S. Farid, Chem. Phys. 176 (1993) 439.
[10] R. Crutchley, Adv. Inorg. Chem. 41 (1994) 273.
[11] C. Creutz, M.D. Newton, N. Sutin, J. Photochem. Photobiol. A: Chem. 82 (1994) 47.
[12] P.F. Barbara, T.J. Meyer, M. Ratner, J. Phys. Chem. 100 (1996) 13148.
[13] P. Piotrowiak, in: V. Balzani (Ed.), Electron Transfer in Chemistry, Wiley-VCH, Weinheim, Germany, 2001.
[14] J.F. Endicott, in: J. McCleverty, T.J. Meyer (Eds.), Comprehensive Coordination Chemistry II, Pergamon, Oxford, UK, 2003.
[15] R.A. Marcus, Discuss. Faraday Soc. 29 (1960) 21.
[16] R. Englman, J. Jortner, Mol. Phys. 18 (1970) 145.
[17] K.F. Freed, J. Jortner, J. Chem. Phys. 52 (1970) 6272.
[18] N. Kestner, J. Logan, J. Jortner, J. Phys. Chem. 64 (1974) 2148.
[19] M. Bixon, J. Jortner, J. Cortes, H. Heitele, M.E. Michel-Beyerle, J. Phys. Chem. 98 (1994) 7289.
[20] J.V. Casper, E.M. Kober, B.P. Sullivan, T.J. Meyer, J. Am. Chem. Soc. 104 (1982) 630.
[21] J.C. Curtis, B.P. Sullivan, T.J. Meyer, Inorg. Chem. 22 (1983) 224.
[22] T.J. Meyer, Prog. Inorg. Chem. 30 (1983) 389.
[23] E.M. Kober, T.J. Meyer, Inorg. Chem. 24 (1985) 106.
[24] E.M. Kober, J.V. Casper, R.S. Lumpkin, T.J. Meyer, J. Phys. Chem. 90 (1986) 3722.
[25] D. Graff, J.P. Claude, T.J. Meyer, in: S.S. Isied (Ed.), Electron Transfer Reactions: Inorganic, Organometallic and Biological Applications, American Chemical Society, Washington, 1997.
[26] D.G. Thompson, J.R. Schoonover, C.J. Timpson, T.J. Meyer, J. Phys. Chem. A 107 (2003) 10250.
[27] A.B. Myers, R.A. Mathies, in: T.G. Spiro (Ed.), Biological Applications of Raman Spectroscopy, Wiley, New York, 1982.
[28] A.B. Myers, Chem. Phys. 180 (1994) 215.
[29] A.B. Myers, Chem. Rev. 96 (1996) 911.
[30] A.B. Myers, Acc. Chem. Res. 30 (1997) 519.
[31] H. Yersin, D. Braun, G. Hensler, E. Galhuber, in: C.D. Flint (Ed.), Vibronic Processes in Inorganic Chemistry, Kluwer, Dordrecht, 1989.
[32] P. Xie, Y.-J. Chen, M.J. Uddin, J.F. Endicott, J. Phys. Chem. A 109 (2005) 4671.
[33] J.F. Endicott, Y.-J. Chen, P. Xie, Coord. Chem. Rev. 249 (2005) 343.
[34] A.B. Myers, in: A.B. Myers, T.R. Rizzo (Eds.), Laser Techniques in Chemistry, John Wiley & Sons Inc., 1995.
[35] J.T. Yardley, Introduction to Molecular Energy Transfer, Academic, New York, NY, 1980.
[36] C.A. Parker, Photoluminescence in Solutions, Elsevier, Amsterdam, The Netherlands, 1968.
[37] J.B. Birks, Photophysics of Aromatic Molecules, Wiley-Interscience, New York, 1970.
[38] R.J. Cave, M.D. Newton, Chem. Phys. Lett. 249 (1996) 15.
[39] Y.-J. Chen, P. Xie, P.G. McNamara, J.F. Endicott, in preparation.
[40] J.T. Hupp, R.T. Williams, Acc. Chem. Res. 34 (2001) 808.
[41] R.D. Cannon, Adv. Inorg. Chem. Radiochem. 21 (1979) 179.
[42] A.B.P. Lever, E. Dodsworth, in: A.B.P. Lever, E.I. Solomon (Eds.), Electronic Structure and Spectroscopy of Inorganic Compounds, vol. II, Wiley, New York, 1999.
[43] J.F. Endicott, in: V. Balzani (Ed.), Electron Transfer in Chemistry, vol. 1, Wiley-VCH, New York, 2001.

[44] D.S. Seneviratne, M.J. Uddin, V. Swayambunathan, H.B. Schlegel, J.F. Endicott, Inorg. Chem. 41 (2002) 1502.
[45] A.B.P. Lever, S.I. Gorelsky, Coord. Chem. Rev. 208 (2000) 153.
[46] K. Maruszewski, K. Bajdor, D.P. Strommen, J.R. Kincaid, J. Phys. Chem. 99 (1995) 6286.
[47] E.I. Solomon, Comments Inorg. Chem. 3 (1984) 225.
[48] T.C. Brunold, H.U. Gudel, in: E.I. Solomon, A.B.P. Lever (Eds.), Inorganic Electronic Structure and Spectroscopy, Wiley-Interscience, New York, 1999.
[49] Y.-J. Chen, P. Xie, J.F. Endicott, J. Phys. Chem. A 108 (2004) 5041.
[50] Y.-J. Chen, P. Xie, J.F. Endicott, O.S. Odongo, J. Phys. Chem. A 110 (2006) 7970.
[51] C.D. Flint, P. Greenough, J. Chem. Soc., Faraday Trans. II 70 (1974) 815.
[52] C.D. Flint, J. Chem. Soc., Faraday Trans. II 72 (1976) 721.
[53] J.F. Endicott, T. Ramasami, R. Tamilarasan, R.B. Lessard, C.K. Ryu, G.B. Brubaker, Coord. Chem. Rev. 77 (1987) 1.
[54] J.F. Endicott, M.W. Perkovic, M.J. Heeg, C.K. Ryu, D. Thompson, in: S.S. Isied (Ed.), Electron Transfer Reactions: Inorganic, Organometallic and Biological Applications, American Chemical Society, Washington, DC, 1997.
[55] D.V. Matyushov, G.A. Voth, J. Phys. Chem. A 104 (2000) 6470.
[56] D.V. Matyushov, M.D. Newton, J. Phys. Chem. A 105 (2001) 8516.
[57] J.F. Endicott, M.J. Uddin, H.B. Schlegel, Res. Chem. Intermed. 28 (2002) 761.
[58] B.J. Coe, J.A. Harris, B.S. Brunschwig, I. Asselberghs, K. Clays, J. Garin, J. Orduna, J. Am. Chem. Soc. 127 (2005) 13399.
[59] P. Xie, Y.-J. Chen, J.F. Endicott, M.J. Uddin, D. Seneviratne, P.G. McNamara, Inorg. Chem. 42 (2003) 5040.
[60] A.B.P. Lever, Inorganic Electronic Spectroscopy, Elsevier, Amsterdam, 1984.
[61] A.B.P. Lever, S.I. Gorelsky, Struct. Bond. 107 (2004) 77.
[62] P.C. Ford, in: M.S. Wrighton (Ed.), Inorganic and Organometallic Photochemistry, American Chemical Society, Washington, DC, 1978.
[63] K. Maruszewski, D.P. Stromen, J.R. Kincaid, J. Am. Chem. Soc. 115 (1993) 8345.
[64] K. Maruszewski, J.R. Kincaid, Inorg. Chem. 34 (1995) 2002.
[65] M. Sykora, J.R. Kincaid, Inorg. Chem. 34 (1995) 5852.
[66] K. Hakamata, A. Urushiyama, H. Kupka, J. Phys. Chem. 85 (1981) 1983.
[67] B.N. Figgis, M.A. Hitchman, Ligand Field Theory and its Applications, Wiley-VCH, New York, 2000.
[68] L.G. Vanquickenbourne, A. Ceulemans, Coord. Chem. Rev. 100 (1983) 157.
[69] C.K. Ryu, J.F. Endicott, Inorg. Chem. 27 (1987) 2203.
[70] Y.-J. Chen, J.F. Endicott, V. Swayambunathan, Chem. Phys. 79 (2006) 326.
[71] E. Krausz, Chem. Phys. Lett. 135 (1987) 249.
[72] E. Krausz, J. Ferguson, Prog. Inorg. Chem. 37 (1989) 293.
[73] H. Yersin, W. Humbs, J. Strasser, Coord. Chem. Rev. 159 (1997) 325.
[74] H. Yersin, D. Braun, Chem. Phys. Lett. 179 (1991) 85.
[75] H.M. McConnell, J. Chem. Phys. 35 (1961) 508.
[76] M.D. Newton, Chem. Rev. 91 (1991) 767.
[77] D.P. Stromen, P.K. Mallick, G.D. Danzer, R.S. Lumpkin, J.R. Kincaid, J. Phys. Chem. 94 (1990) 1357.
[78] Y.K. Shin, D.J. Szalda, B.S. Brunschwig, C. Creutz, N. Sutin, Inorg. Chem. 36 (1997) 3190.
[79] Y.-J. Chen, P. Xie, M.J. Heeg, J.F. Endicott, Inorg. Chem., ASAP (2006) 6282.
[80] H. Kobayashi, Y. Kaizu, Coord. Chem. Rev. 64 (1985) 53.
[81] P. Egger, J. Hulliger, Coord. Chem. Rev. 183 (1999) 101.
[82] J.F. Endicott, P.G. McNamara, T. Buranda, A.V. Macatangay, Coord. Chem. Rev. 208 (2000) 61.
[83] K. Nakamoto, Infrared and Raman Spectra of Inorganic and Coordination Compounds. Part B; Wiley, New York, 1997.
[84] J.F. Endicott, J.Y. Chen, Inorg. Chim. Acta, in press.
[85] M.A. Watzky, J.F. Endicott, X. Song, Y. Lei, A.V. Macatangay, Inorg. Chem. 35 (1996) 3463.
[86] M.A. Watzky, A.V. Macatangay, R.A. Van Camp, S.E. Mazzetto, X. Song, J.F. Endicott, T. Buranda, J. Phys. Chem. 101 (1997) 8441.
[87] J.F. Endicott, M.A. Watzky, X. Song, T. Buranda, Coord. Chem. Rev. 159 (1997) 295.
[88] J.F. Endicott, X. Song, M.A. Watzky, T. Buranda, J. Photochem. Photobiol. A: Chem. 82 (1994) 181.
[89] J.F. Endicott, X. Song, M.A. Watzky, T. Buranda, Chem. Phys. 176 (1993) 427.
[90] C.K. Ryu, R.B. Lessard, D. Lynch, J.F. Endicott, J. Phys. Chem. 93 (1989) 1752.
[91] C.K. Ryu, J.F. Endicott, Inorg. Chem. 27 (1988) 2203.
[92] R.B. Lessard, J.F. Endicott, M.W. Perkovic, L.A. Ochrymowycz, Inorg. Chem. 28 (1989) 2574.
[93] R.B. Lessard, M.J. Heeg, T. Buranda, M.W. Perkovic, C.L. Schwarz, Y. Rudong, J.F. Endicott, Inorg. Chem. 31 (1992) 3091.
[94] J.F. Endicott, R.B. Lessard, Y. Lei, C.K. Ryu, in: V. Balzani (Ed.), Supramolecular Photochemistry, D. Reidel, Dordrecht, 1987.
[95] C.A. Bignozzi, O. Bortolini, C. Chiorboli, M.T. Indelli, M.A. Rampi, F. Scandola, Inorg. Chem. 31 (1992) 172.
[96] R.B. Wilson, E.I. Solomon, Inorg. Chem. 17 (1978) 1729.
[97] R.B. Wilson, E.I. Solomon, J. Am. Chem. Soc. 102 (1980) 4085.
[98] M.D. Newton, N. Sutin, Annu. Rev. Phys. Chem. 35 (1984) 437.
[99] R.A. Marcus, N. Sutin, Biochem. Biophys. Acta 811 (1985) 265.
[100] R.W. Callahan, F.R. Keene, T.J. Meyer, D.J. Salmon, J. Am. Chem. Soc. 99 (1977) 1064.
[101] M.J. Powers, T.J. Meyer, J. Am. Chem. Soc. 102 (1980) 1289.
[102] J.V. Casper, T.J. Meyer, Inorg. Chem. 22 (1983) 2446.
[103] E.M. Kober, J.M. Marshall, W.J. Dressick, B.P. Sullivan, J.V. Caspar, T.J. Meyer, Inorg. Chem. 24 (1985) 2755.
[104] P. Chen, T.J. Meyer, Chem. Rev. 98 (1998) 1439.
[105] K.D. Demadis, E.-S. El-Samanody, G.M. Cola, T.J. Meyer, J. Am. Chem. Soc. 121 (1999) 535.
[106] K.D. Demadis, C.M. Hartshorn, T.J. Meyer, Chem. Rev. 101 (2001) 2655.

Glossary

trien: triethylenetetraamine
[12]aneN$_4$: 1,4,7,10-tetraazacyclododecane
[14]aneN$_4$: 1,4,8,11-tetraazacyclotetradecane
rac-Me$_6$[14]aneN$_4$: 5,12-*rac*-5,7,7,12,14,14-hexamethyl-1,4,8,11-tetraazacyclotetradecane
m-Me$_6$[14]aneN$_4$: 5,12-*meso*-5,7,7,12,14,14-hexamethyl-1,4,8,11-tetraazacyclotetradecane
pyo[14]eneN$_4$: *meso*-2,12-dimethyl-3,7,11,14-tetraazabicyclo[11.3.1]heptadeca-1(17)-aneN$_4$
[15]aneN$_4$: 1,4,8,12-tetraazacyclopentadecane
bpy: 2,2′-bipyridine
dpp: 2,3-bis-(2-pyridyl)pyrazine
dpq: 2,3-bis(2-pyridyl)quinoxaline
dpb: 2,3-bis(2-pyridyl)benzoquinoxaline
bpm: 2,2′-dipyrimidine.